frontiers in Marine Science

ORIGINAL RESEARCH
published: 19 August 2021
doi: 10.3389/fmars.2021.699762

New Constraints on the Physical and Biological Controls on the Silicon Isotopic Composition of the Arctic Ocean

Mark A. Brzezinski[1,2], Ivia Closset[1], Janice L. Jones[1], Gregory F. de Souza[3] and Colin Maden[3]*

[1] Marine Science Institute, University of California, Santa Barbara, Santa Barbara, CA, United States, [2] Department of Ecology Evolution and Marine Biology, University of California, Santa Barbara, Santa Barbara, CA, United States, [3] Institute of Geochemistry and Petrology, ETH Zürich, Zurich, Switzerland

The silicon isotope composition of silicic acid, $\delta^{30}Si(OH)_4$, in the deep Arctic Ocean is anomalously heavy compared to all other deep ocean basins. To further evaluate the mechanisms leading to this condition, $\delta^{30}Si(OH)_4$ was examined on US GEOTRACES section GN01 from the Bering Strait to the North Pole. Isotope values in the polar mixed layer showed a strong influence of the transpolar drift. Drift waters contained relatively high $[Si(OH)_4]$ with heavy $\delta^{30}Si(OH)_4$ consistent with the high silicate of riverine source waters and strong biological $Si(OH)_4$ consumption on the Eurasian shelves. The maximum in silicic acid concentration, $[Si(OH)_4]$, within the double halocline of the Canada Basin formed a local minimum in $\delta^{30}Si(OH)_4$ that extended across the Canada Basin, reflecting the high-$[Si(OH)_4]$ Pacific source waters and benthic inputs of $Si(OH)_4$ in the Chukchi Sea. $\delta^{30}Si(OH)_4$ became lighter with the increase in $[Si(OH)_4]$ in intermediate and deep waters; however, both Canada Basin deep water and Eurasian Basin deep water were heavier than deep waters from other ocean basins. A preliminary isotope budget incorporating all available Arctic $\delta^{30}Si(OH)_4$ data confirms the importance of isotopically heavy inflows in creating the anomalous deep Arctic Si isotope signature, but also reveals a surprising similarity in the isotopic composition of the major inflows compared to outflows across the main gateways connecting the Arctic with the Pacific and the Atlantic. This similarity implies a major role of biological productivity and opal burial in removing light isotopes entering the Arctic Ocean from rivers.

Keywords: nutrients, biogeochemical cycles, diatoms, silicon isotopes, Arctic Ocean, GEOTRACES, stable isotope Si30

OPEN ACCESS

Edited by:
Sunil Kumar Singh, Physical Research Laboratory, India

Reviewed by:
Christian März, University of Leeds, United Kingdom
Georgi Laukert, GEOMAR Helmholtz Center for Ocean Research Kiel, Germany

****Correspondence:***
Mark A. Brzezinski
mark.brzezinski@ucsb.edu

Specialty section:
This article was submitted to Marine Biogeochemistry, a section of the journal Frontiers in Marine Science

Received: *24 April 2021*
Accepted: *23 June 2021*
Published: *19 August 2021*

Citation:
Brzezinski MA, Closset I, Jones JL, de Souza GF and Maden C (2021) New Constraints on the Physical and Biological Controls on the Silicon Isotopic Composition of the Arctic Ocean. Front. Mar. Sci. 8:699762. doi: 10.3389/fmars.2021.699762

INTRODUCTION

Silicon is an essential nutrient for the growth of diatoms and other siliceous plankton. Diatoms are thought to dominate the marine silicon cycle and they account for up to 30% of global marine primary production (Tréguer et al., 2021) creating a strong link between diatom Si demand (Lewin, 1962) and the global carbon cycle (Nelson et al., 1991; Tréguer and van Bennekom, 1991; Nelson and Brzezinski, 1997; Brzezinski et al., 1998, 2001). The discovery that diatoms fractionate isotopes

of Si during silicification (De La Rocha et al., 1997) led to natural variations in the isotopic composition of Si becoming a new tool that expanded the spatial and temporal scales for assessing diatom silica production and productivity in the present (e.g., Fripiat et al., 2011) and in the past (e.g., De La Rocha et al., 1998) and their implications for climate (De La Rocha et al., 1998; Beucher et al., 2007; Hendry and Brzezinski, 2014; Dumont et al., 2020).

The isotope models used to infer silica production from the Si isotope composition of diatom frustules in marine sediment or from the water column all depend on knowledge of the isotopic composition of the silicic acid, $\delta^{30}Si(OH)_4$, in upwelling water masses (Varela et al., 2004). That dependence inspired efforts to understand ties between Si isotope dynamics and the meridional overturning circulation (de Souza et al., 2012a; Brzezinski and Jones, 2015; Closset et al., 2016; Sutton et al., 2018). Numerical models that combine large-scale ocean circulation with biological fractionation of isotopes of Si in surface waters together with the dissolution of biogenic silica (bSi) in the water column are able to simulate global Si isotope distributions with high skill (Reynolds, 2009; de Souza et al., 2014, 2015; Holzer and Brzezinski, 2015; Gao et al., 2016) suggesting that this relatively simple conceptual framework captures the main relevant processes.

The silicon isotope composition of the deep waters of the Canada, Makarov, and Amundsen Basins (**Figure 1**) are all heavy relative to the rest of the global ocean (Varela et al., 2016; Liguori et al., 2020). The mechanisms leading to a heavy silicon isotopic signature of the deep Arctic Ocean remain unclear. Varela et al. (2016) proposed that the relatively shallow sills that separate the Arctic Ocean from the Atlantic and Pacific Oceans (Rudels, 2009) play a major role. Because Si isotope values are generally inversely related to silicic acid concentration throughout the ocean (Cardinal et al., 2005; de Souza et al., 2014; Brzezinski and Jones, 2015). Si isotope values become progressively heavier toward the surface in the upper 2 km of the water column following the decrease in silicic acid concentration through the main thermocline. Thus shallow sills increase the contribution of heavy signals from shallower layers and restrict connectivity with lighter deep waters. Varela et al. (2016) evaluated their hypothesis using a simple box model of the global ocean that successfully simulated a heavy Si isotopic composition for the deep Arctic compared to other ocean basins.

A study of Si isotopes focused on the Eurasian Basin by Liguori et al. (2020) revealed the importance of water mass mixing as a major control on Si isotope distributions within the central Arctic Ocean. Liguori et al. (2020) argue that water mass mixing plays a larger role in Si isotope dynamics within the Arctic Ocean than do processes associated with bSi production and dissolution. That argument is consistent with the low rates of productivity and low bSi concentrations in the Arctic (Fahl and Nöthig, 2007) and the strong role of processes on the shelves in the formation of halocline, intermediate, and deep waters of the central Arctic (Schauer et al., 2002; Rudels, 2009, 2012). The redistribution of isotopes of Si within the Arctic Ocean with the formation and mixing of water masses has important consequences for the isotopic composition of major Arctic outflows that influence the composition of North Atlantic deep water, NADW. Outflows from the Canada Basin through the Canadian Archipelago and Davis Strait influence the composition of Labrador Sea water (LSW), while outflows from the Eurasian Basin through the Fram Strait flow into the Greenland and Norwegian Seas are incorporated into overflow waters through the Denmark Strait (DSOW) and Iceland Scotland Ridge (ISOW; Dickson and Brown, 1994). Liguori et al. (2020) point to differences in $\delta^{30}Si(OH)_4$ reported for the Canada, Makarov and Amundsen Basins to suggest that these outflows contribute a diversity of end-member isotopic compositions to NADW.

Evaluating both the effect of inflows on Arctic Ocean Si isotope distribution and the influence of the Arctic Ocean outflows on NADW composition is currently difficult due to the lack of information on the isotopic composition of end member water masses entering or leaving the Arctic Ocean. Only a few $\delta^{30}Si(OH)_4$ measurements are available for inflows of Pacific Ocean water through the Bering Strait (Giesbrecht, 2019) and measurements are completely lacking for Atlantic Ocean waters that enter through the Fram Strait and over the Barents Sea. Giesbrecht (2019) provides values for the isotopic composition of outflows through the Canadian Archipelago and the Davis Strait that influence LSW, but no data are available for outflows through the Fram Strait that ultimately influence the composition of ISOW and DSOW. Measurements of the isotopic composition of overflow waters are available (de Souza et al., 2012b; Sutton et al., 2018), but mechanistically linking their composition back to the diversity of isotope compositions of Arctic Ocean water masses is currently difficult (Liguori et al., 2020).

The US GEOTRACES expedition, GN01, offered an opportunity to further test and develop these concepts by expanding the Si isotope data set in the Amerasian Basin of the Arctic Ocean, including sampling of the isotopic composition of Pacific inflows through the Bering Strait. Comparison with previous data sets allows a more comprehensive analysis of the relative importance of physical and biological processes in controlling $\delta^{30}Si(OH)_4$ in the central Arctic and the construction of a preliminary Si isotope budget for the Arctic Ocean.

MATERIALS AND METHODS

Sample Collection

Seawater samples for $\delta^{30}Si(OH)_4$ measurement were collected from 15 of the 66 stations sampled during GEOTRACES section GN01 aboard the icebreaker *CGC* Healy (HLY1502) from August to October, 2015 (**Figure 1**). After sampling in the Bering Strait and Chukchi Sea, sample collection generally followed a westerly meridian to the North Pole and then returned to the Canadian margin following a more easterly meridian (**Figure 1**). All samples were collected using the conventional GEOTRACES rosette/CTD package that included a 24 – place rosette fitted with 12 – liter Niskin bottles. Three liters of seawater were filtered directly from each Niskin sampler through silicone tubing using a trace – metal – grade HCl – rinsed inline AcroPak® 500 capsule filter containing dual 0.8 and 0.45 μm Supor membrane filters. Capsule filters and collection bottles were well rinsed with sample water prior to sample collection. Filled sample bottles were tightly

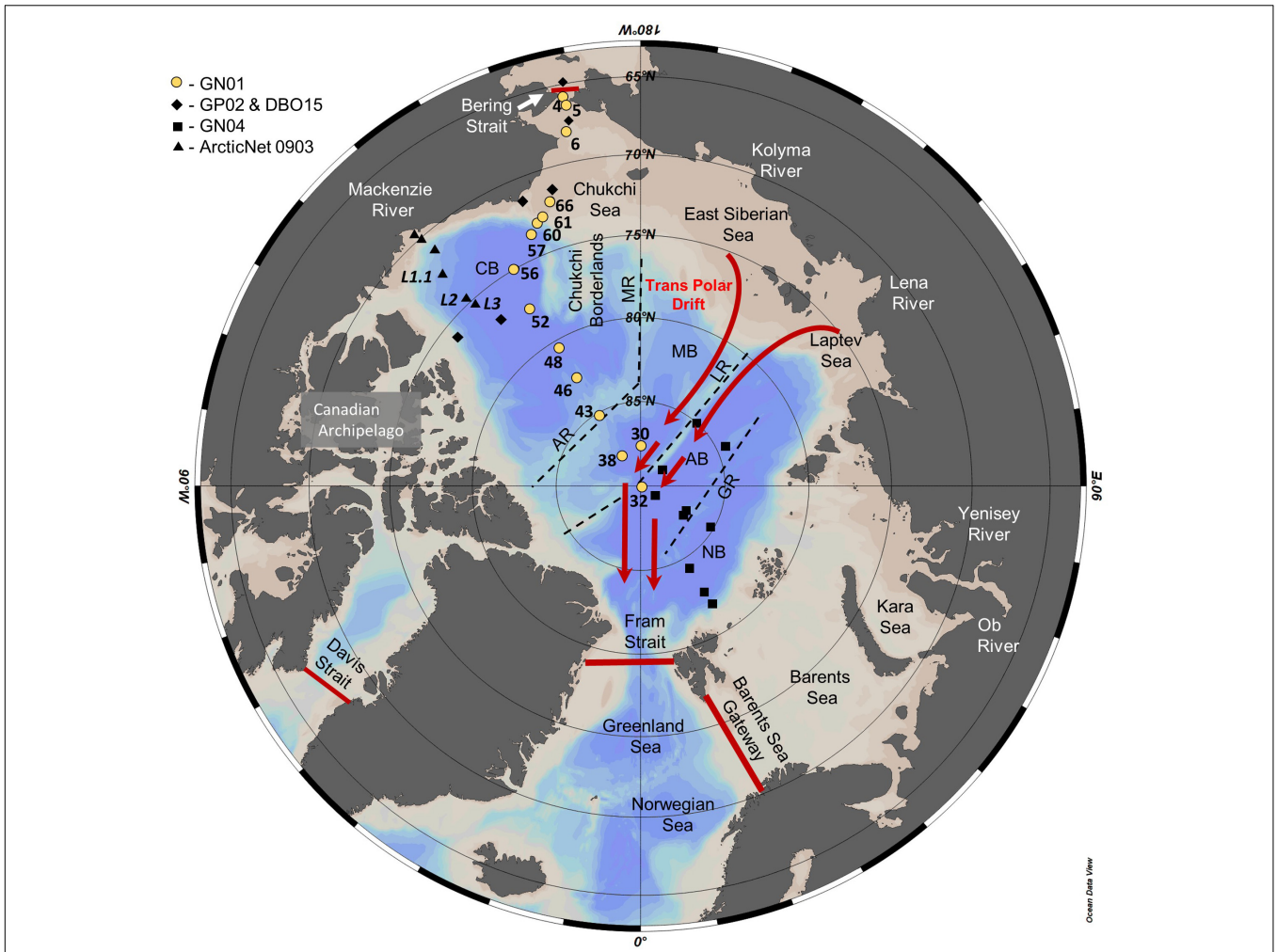

FIGURE 1 | Map of the Arctic Ocean showing the location of stations sampled during US GEOTRACES GN01, Canadian GEOTRACES GP02 and Canadian Distributed Biological Observatory cruise DBO15, German GEOTRACES GN04, and Canadian IPY-GEOTRACES (ArcticNet 0903). Red lines denote major exchange gateways of the Bering Strait, Davis Strait, Fram Strait, and Barents Sea used to determine the Arctic Ocean silicic acid budget (Torres-Valdés et al., 2013). Dotted lines approximate the position of the Alpha and Mendeleev Ridge (AR and MR) separating the Canada Basin (CB) and the Makarov Basin (MB), the Lomonosov Ridge (LR) separating the Makarov Basin and the Amundsen Basin (AB), and the Gakkel Ridge (GR) separating the Amundsen Basin and the Nansen Basin (NB). Red arrows indicate the approximate flow path of the transpolar drift (TPD).

capped and stored at room temperature without preservative. AcroPak capsule filters were kept refrigerated between samplings and replaced periodically.

Sample Processing

For most samples the silicic acid within seawater was prepared for Si isotope analysis by conversion to $BaSiF_6$. Briefly, subsamples containing 5–30 μmol of Si were reacted with triethylamine-ammonium molybdate to precipitate the silicic acid as triethyamine-silicomolybdic acid (De La Rocha et al., 1996; Brzezinski et al., 2006). The precipitate was collected by filtration, rinsed, dried, and combusted to form solid SiO_2. The SiO_2 was then dissolved in HF and precipitated as Cs_2SiF_6 by the addition of CsCl (Brzezinski et al., 2006). The precipitate was rinsed with ethanol and dried. Then a solution of $BaCl_2$ was added and left for 48 h to allow for quantitative conversion of Cs_2SiF_6 to $BaSiF_6$. $BaSiF_6$ was similarly rinsed and dried and its isotopic composition analyzed through thermal decomposition of $BaSiF_6$ to solid BaF_2 and SiF_4 gas using a NuSil inlet system coupled to a Nu Perspective IRMS mass spectrometer at the University of California Santa Barbara (UCSB). Si isotopes were measured as SiF_3^+ ions produced by electron bombardment of SiF_4 gas at *m/z* 85, 86, and 87. The secondary standards, Big Batch and Diatomite, and the NIST primary standard NBS-28 (RM8546), were analyzed at the start and end of every run of 50 samples. The reference seawater $ALOHA_{1,000}$ (Grasse et al., 2017) was included in nearly every run. Seawater samples were analyzed in duplicate or triplicate with each analysis performed on a separate analytical run of the mass spectrometer.

Isotope values were calibrated against the international standard NBS28 and the well-characterized secondary standards Big Batch and Diatomite (Reynolds et al., 2007;

Grasse et al., 2017) using the multipoint calibration method of Paul et al. (2007). For calibration, the measured $\delta^{30}Si$ values for all three reference materials ($\delta^{30}Si_{measured}$) are regressed against their consensus $\delta^{30}Si$ values with NSB = 0‰, Big Batch = −10.48‰, and Diatomite = + 1.26‰ (Reynolds et al., 2007). Standardized sample values are calculated from the regression line:

$$\delta^{30}Si = \text{slope} \times \delta^{30}Si_{\text{measured}} + \text{intercept} \quad (1)$$

The regression approach produces a smaller normalization error than the single-point normalization to NBS28 as it is more robust against random error in the analysis of any one standard (Paul et al., 2007). In the multipoint regression approach, the value obtained for NBS is dictated by the regression rather than being assumed to be zero as done in the single – standard approach using NBS28. The regression approach for 20 randomly chosen calibrations predicts a value of NBS of +0.03 ± 0.01‰ ($1\sigma_{SE} = 1\sigma_{SD} \div n^{1/2}$; unless otherwise labeled all uncertainty terms hereafter are standard errors, $1\sigma_{SE}$, corresponding to our best estimate of the uncertainty on our estimate of the true population mean) compared to the assigned value of zero with the difference being well within the analytical precision of current single-sample $\delta^{30}Si$ measurements (Reynolds et al., 2007; Grasse et al., 2017).

Low concentration samples with <5 μmol kg^{-1} silicic acid along with nine intercalibration samples with 13–40 μmol kg^{-1} silicic acid were processed and analyzed at the Swiss Federal Institute of Technology (Eidgenössische Technische Hochschule, ETH) Zurich, Switzerland following the methods of Reynolds et al. (2006) and Georg et al. (2006) as modified by de Souza et al. (2012b). Briefly, Si was pre-concentrated from 13 to 150 mL of seawater by inducing the precipitation of seawater Mg as brucite, $Mg(OH)_2$, through addition of NaOH (Suprapur, Merck); the resulting scavenging of Si onto the brucite allows separation of the analyte from the bulk of seawater salts by centrifugation. For samples with Si concentrations below 14 μmol kg^{-1}, the brucite pellet was re-dissolved in a small volume of fresh sample and the pre-concentration procedure repeated. Yields of the procedure, monitored by photospectrometric analysis of Si concentrations in the supernatant after centrifugation, were always ≥97.65% and were generally ∼99%. Following dissolution of the brucite pellet by addition of double-distilled 6 M HCl, samples were diluted with ultrapure water (≥18.2 MΩ cm) to 1.8 ppm Si, and Si separated from Mg and other seawater cations by passing the solution through a chromatographic column containing 1 mL of the cation-exchange resin AG50W-X8 (BioRad Laboratories). The resulting solutions, with a concentration of 0.6 ppm Si, were analyzed by high-resolution multicollector-ICP-MS (NuPlasma 1700) using a standard – sample bracketing protocol (Georg et al., 2006). Each $\delta^{30}Si$ analysis comprises five measurements (each consisting of 1 block of 36 × 5 s integrations) of the isotopic ratios in the sample bracketed by measurements of the isotopic ratios in the primary isotopic standard NBS28 (seven measurements of NBS28). Secondary standards and reference materials were analyzed with each batch of samples to monitor accuracy and provide an estimate of external reproducibility.

Seawater nutrient analyses (phosphate, silicate, nitrate + nitrite, and nitrite) were performed at sea on a Seal Analytical continuous-flow Auto Analyzer 3 following Hydes et al. (2010).

ANALYTICAL PRECISION AND INTERCALIBRATION

Reference Materials and Sample Precision

The analysis of secondary standards at both UCSB and ETH gave values that were all within 0.06‰ or better compared to consensus values. The analysis of the secondary standard Diatomite at UCSB and ETH gave values of +1.24 ± 0.01‰ (n = 73) and +1.28 ± 0.07‰ (1σ, n = 1), respectively, in good agreement with the consensus value of +1.26 ± 0.01‰ (Reynolds et al., 2007). Analysis of the Big Batch standard at UCSB gave a mean value of −10.42 ± 0.01‰ (n = 118), compared to the consensus value of −10.48 ± 0.02‰ (Reynolds et al., 2007). The sponge spicule secondary standard LMG08 was analyzed at EH yielding a mean value of −3.36 ± 0.02‰ (n = 8) versus the consensus value of −3.37 ± 0.02‰ (Hendry et al., 2011). Long-term external reproducibility at ETH is documented by analyses of Diatomite over a period of ∼2 year preceding the analyses reported here, which yields +1.26 ± 0.07‰ (1σ, n = 32).

Both UCSB and ETH analyzed the reference seawater $ALOHA_{1,000}$ yielding an average value of +1.29 ± 0.01‰, n = 44 at UCSB and +1.26 ± 0.02‰, n = 7 at ETH with both values being slightly heavier than the consensus value of +1.24 ± 0.03‰ (Grasse et al., 2017). Seawater samples measured by each laboratory had excellent and similar precision. Replicates at UCSB had an average precision of 0.05‰ (min = 0.0001‰, max 0.20‰, 2 σ_{SD} = 0.06‰, and n = 203). The low silicic acid concentration samples measured at ETH had an average precision of 0.08‰ (min = 0.04‰, max 0.15‰, 2 σ_{SD} = 0.06‰, and n = 27). When averaging across several samples, e.g., for determination of water mass averages, the associated error of the average was always taken to be the larger of $1\sigma_{SDsamples} \div n^{1/2}$ or $1\sigma_{SD\_ALOHA} \div n^{1/2}$, where n is the number of samples averaged, such that errors are not underestimated in cases where $1\sigma_{SD\_samples}$ is small by coincidence.

Crossover Stations and Intercalibration

To intercalibrate the results from UCSB and ETH nine samples from four stations along GN01 (stations 32: 1 sample, 46: 3 samples, 52: 3 samples, and 57: 2 samples) that had silicic acid concentrations between 13 and 40 μmol kg^{-1} were analyzed by both laboratories. The average of the absolute value of the differences in $\delta^{30}Si$ values for these samples was 0.03 ± 0.01‰ ($1\sigma_{SE}$, n = 9). The high variance relative to the mean is due to a single difference of 0.13‰. The median difference that is less sensitive to this outlier was 0.016‰.

Two crossover stations with other GEOTRACES cruises were occupied for intercalibration during GN01. Station 56 of GN01 (75°N, 148.8°E; 29 September 2015, **Figure 1**) was also

occupied by *CCGS* Amundsen during Canadian GEOTRACES cruise GN03 (Station CB4, 15 September 2015), just 14 days earlier. Samples from GN03 were collected by the University of Victoria, Canada (D. Varela/K. Giesbrecht) and analyzed at ETH Zurich. The second crossover station was GN01 Station 30 (87.5°N, 180°E; 01/02 September 2015, **Figure 1**) in the Makarov Basin, occupied about 10 days later during GN04 aboard the *FS* Polarstern, PS94 (Station 101, 13/14 September 2015). Samples from PS94 were analyzed at the University of Oldenburg, Germany (C. Ehlert). Samples from GN01 crossover stations were analyzed by the University of California Santa Barbara, United States (M. Brzezinski) and are presented in this study.

Technical difficulties during GN01 restricted sampling at crossover station GN01 56 (GN03 station CB4) to depths below 600 m. The $\delta^{30}Si(OH)_4$ data from the two laboratories are in excellent agreement, with an average of the absolute differences between laboratories of 0.13 ± 0.08‰ ($1\sigma_{SE}$, n = 4) when all data are paired by closest common depth and 0.05 ± 0.03‰ ($1\sigma_{SE}$, n = 3) for samples from waters >1,200 m. Sampling at GN01 Station 30 (GN04 station 101) extended from 20 m to near the sea floor. However, considering the large gradients in isotope values in surface waters (0–200 m) that could bias differences when samples are paired by closest sampling depth, the comparison of crossover station data used samples from >200 m. The $\delta^{30}Si(OH)_4$ data analyzed in Oldenburg were always lighter than comparison samples analyzed in Santa Barbara. When the data are paired by the closest common depth sample values differ by 0.17 ± 0.06‰ ($1\sigma_{SE}$, n = 12) for all samples below 200 m and by 0.18 ± 0.06‰ ($1\sigma_{SE}$, n = 4) for deep waters below 1,200 m. Considering the very short time between sampling of this location on GN01 and GN04 (10 days) natural variations of this magnitude seem unlikely, especially in deep waters. A similar offset of 0.19‰ was observed between these same two laboratories during the international study to establish the ALOHA reference seawaters for isotopes of Si (Grasse et al., 2017). Thus, the offset observed likely reflects inter-laboratory differences resulting from some combination of the different methods used for chemical sample preparation, including preconcentration and purification methods, and isotopic analysis on different mass-spectrometer types, i.e., the Neptune MC-ICP-MS (Thermo Fisher^{TM}, Germany) used, e.g., in Oldenburg, and the NuSil and Nu Perspective IRMS (Nu Instruments, United Kingdom) used in Santa Barbara. We note, however, that the chemical preparation methods used in Oldenburg are identical to those applied at ETH Zurich (where subsequent analysis is by MC-ICP-MS, a NuPlasma 1700) for which excellent agreement with Santa Barbara data was reported above, such that there is likely no single simple cause of such inter-laboratory differences (see also discussion in Grasse et al., 2017).

STUDY SITE

Water Masses and Hydrography

The Arctic Ocean is a semi-enclosed sea with nearly equal areas of shallow shelves and deep basins that receives considerable freshwater input relative to its size (Carmack and Wassmann, 2006; Wassmann, 2015; Carmack et al., 2016; **Figure 1**). Ridges rising from the sea floor divide the Arctic Ocean into a series of sub – basins. The Lomonosov Ridge nearly bisects the central Arctic Ocean, separating the western Amerasian Basin from the eastern Eurasian Basin and restricting free advective exchange between the two to water depths of <1,800 m (Björk and Winsor, 2006). The Alpha and Mendeleev Ridges further subdivide the Amerasian Basin into the Canada and Makarov Basins. The geographic North Pole lies adjacent to the Lomonosov Ridge in the Amundsen Basin on the Eurasian side where the Gakkel Ridge separates the Amundsen and Nansen Basins. Sampling for Si isotopes on GN01 mainly sampled the Canada Basin, with two stations in the Makarov Basin (stations 30, 38) and a single station at the pole in the Amundsen Basin (St 32). Station 43, located above the Alpha Ridge at 2,200 m water depth, displayed hydrographic and nutrient characteristics of the Canada Basin. GN01 did not sample the Nansen Basin (**Figure 1**).

The Bering Strait is the sole connection between the Arctic and Pacific Oceans, while flows through the Canadian Archipelago, Fram Strait, and Barents Sea connect the Arctic and the Atlantic Oceans (**Figure 1**). Exchange through the Bering Strait is restricted by a sill depth of only 50 m. Outflows through the Canadian Archipelago are also relatively shallow (<250 m), as is exchange across the Barents Sea (200–300 m), while the 2,500 m Fram Strait allows deeper communication with the Greenland and Norwegian Seas. The Greenland-Scotland Ridge to the south of the Fram Strait at the southern end of the Norwegian Sea near Iceland (not shown) restricts communication with the North Atlantic to 600–800 m. Overall, Arctic Ocean circulation bears similarity to that of the Mediterranean Sea with deep waters having only limited communication with the Atlantic Ocean through the Fram Strait and no direct exchange with the Pacific.

Advection of the Arctic inflows, their mixing and their interaction with freshwater inflows and shelf sediments influences biogeochemical properties in both the Amerasian and Eurasian Basins. A key hydrographic feature that dictates water mass dynamics in the Arctic Ocean is the strong shallow halocline present in the upper 100–300 m that extends across the central Arctic Ocean. Halocline waters form on the shelves, increasing in salinity and density due to brine rejection during sea ice formation, thus creating a strong link between shelf processes and the hydrography of the central Arctic Ocean. The halocline prevents deep convection such that lateral advection through the subduction of inflows modified by sea ice formation on the shelves plays a major role in deep water ventilation of the central Arctic Ocean (Rudels, 2009).

There are several schemes used to define water masses of the Arctic Ocean based on physical and nutrient properties. The definitions used here are presented in **Table 1**. We adopt the scheme of Rudels (2009, 2012) for deeper waters to be consistent with Si isotope data published for the Eurasian Basin by Liguori et al. (2020). The scheme of Jensen et al. (2019) is adopted for shallower waters including the halocline. Stations in the Bering Strait and Chukchi Sea (<70 m water depth) are classified separately from the other stations that sampled deep basins.

TABLE 1 | Water mass definitions.

Water mass	Abbreviation	Definition
Shelf waters		
Bering Strait	BS	Latitude < 66.5°N Bottom depth < 60 m
Chukchi Sea	CS	Latitude > 66.5°N Bottom depth < 75 m
Surface waters		
Polar mixed layer	PML	$\sigma_\theta \leq 27.7$ bottom depth > 800 m
Polar mixed layer (Trans polar drift)	TPD	Latitude > 84°N % meteoric water ≈ 15% CDOM ≈ 0.13 V z < 60 m
Halocline waters		
Canada Basin		
Upper halocline layer	UHL	θ = −1.5 to +0.4°C S = 31.0 to 33.1 [Si] <18 μmol kg^{-1}
Upper halocline layer (Pacific)	UHLP	θ = −1.5 to +0.4°C S = 31.0 to 33.1 [Si] >18 μmol kg^{-1}
Lower halocline layer	LHL	θ = −1.5 to +0.3°C S = 33.1 to 34.7
Makarov Basin		
Halocline layer	HM	θ = −1.5 to +0.7°C S = 31.0 to 34.3
Amundsen Basin		
Halocline layer	HA	θ = −1.8 to +1.6°C S = 32.7 to 34.7
Intermediate waters I ($27.7 < \sigma_\theta \leq 27.97$)		
Atlantic water	AW	θ > 2°C
Arctic Atlantic water	AAW	0°C < θ ≤ 2°C
Intermediate waters II ($\sigma_\theta > 27.97$, $\sigma_{0\text{-}5} \leq 30.444$)		
Dense Arctic Atlantic water	DAAW	θ > 0°C
Upper polar deep water	uPDW	θ ≤ 0°C
Deep waters ($\sigma_{0\text{-}5} > 30.444$)		
Eurasian basin deep water	EBDW	θ ≤ −0.6°C S > 34.915
Canada basin deep water	CBDW	θ > −0.6°C S > 34.915

Shelf waters are defined based on geographic location and bottom depth. Surface and halocline waters as described by Jensen et al. (2019) based on Jones and Anderson (1986), Rudels (2012), and Rudels et al. (2015). Transpolar drift surface waters as described in Charette et al. (2020). Intermediate and deep waters as defined by Rudels (2012).

The shallow halocline limits the vertical extent of well – mixed surface waters, known as the polar mixed layer (PML), to the upper 60 m or less. The PML at the more northerly stations sampled on GN01 (>84°N latitude) lies within the transpolar drift (TPD) based on both meteoric water content and CDOM concentration (Shimada et al., 2005; Charette et al., 2020). The Drift carries waters from the Eurasian shelves across the Arctic Ocean where they then exit through the Fram Strait (**Figure 1**).

The structure of the halocline underlying the PML varies among basins as a function of the extent of Pacific water influence. Atlantic waters contribute to the halocline across the entire central Arctic Ocean. In the Canada Basin, water from the Pacific forms an upper halocline that overlies the halocline formed by Atlantic waters, creating a double halocline. This upper halocline layer (UHL) forms in the Chukchi Sea where salt added by brine rejection during sea ice formation increases density (Timmermans et al., 2003; Shimada et al., 2005; Woodgate et al., 2005). The denser waters sink to the depth of the UHL and spreads across much of the Canada Basin.

The Pacific waters of the UHL are distinguished by a subsurface maximum in silicic acid concentration that reflects both the water's origin in the Pacific and the input of regenerated silicic acid from sediments in the shallow Chukchi Sea (Jones and Anderson, 1986; Nishino et al., 2009, 2015; Kipp et al., 2020). For this study, the UHL defined by potential temperature (θ) and salinity (S) is further subdivided based on silicic acid content, with waters containing >18 μmol kg^{-1} silicic acid (twice the average silicic acid concentration in the PML) considered representative of the isotopic composition of the Si maximum associated with Pacific waters in the central Arctic Ocean (denoted as UHLP, **Table 1**). In contrast to the UHL, the Atlantic waters of the lower halocline layer (LHL) in the Canada Basin are modified through brine rejection on the Eurasian shelves, ultimately mixing with water of Pacific origin during subduction in the Canada Basin (Jones and Anderson, 1986).

Intermediate waters in all Arctic Ocean basins originate in the Atlantic Ocean (Woodgate et al., 2001; Schauer et al., 2002). Intermediate waters lie above ridge top depths, allowing inter-basin exchange and lateral mixing. In the Makarov and Canada Basins the Atlantic layer extends from the base of the halocline to about 1,100 m. The Atlantic layer can be further subdivided into a shallow (350–800 m) Fram Strait Branch (FSB; θ > 0°C, S 34.86) and the deeper Barents Sea branch (BSB; θ > −0.15 to 0°C, S 34.88, Woodgate et al., 2001; Schauer et al., 2002). The FSB consists of Atlantic waters that entered the Arctic Ocean through Fram Strait and is warm and fresh compared to the deeper BSB (800–1,150 m) that consists of Atlantic inflows that are altered in the shallow Barents Sea and on Eurasian shelves before subducting to depth.

For the Eurasian Basin, Rudels (2012) defines two layers of intermediate waters each with two sublayers based on density and potential temperature (**Table 1**). Relatively warm Atlantic Water (AW, θ > 2°C) as defined by Rudels (2012) is transformed into Dense Arctic Atlantic Water (DAAW) before reaching the Amerasian basins and was not observed on GN01. Arctic Atlantic Water (AAW) and DAAW occupy the same overall depth range as FSB and BSB, respectively, (Woodgate et al., 2001; Schauer et al., 2002), and were both present along the GN01 section. Upper polar deep water (uPDW) present in the Nansen and Amundsen Basins becomes modified in the Canada and Makarov Basins (Rudels, 2009) and corresponds to the transition layer defined by Swift et al. (1997). Here we maintain the definitions and naming scheme given in **Table 1**, including uPDW, to facilitate comparisons with previously published data on Arctic Si isotope distributions by Liguori et al. (2020).

Deep waters of the Arctic also originate in the Atlantic Ocean. The ridge system restricts exchange among deep basins, leading to increasing water age between Eurasian Basin deep water (EBDW) in the Amundsen Basin (∼250 years), and the

Canada Basin deep water (CBDW) found in both the Makarov (~300 years) and Canada (~400 years) Basins (Schlosser et al., 1997; Tanhua et al., 2009). EBDW is slightly colder and fresher than is CBDW due to a stronger influence from the Nordic Seas (Rudels, 2009). GN01 sampled EBDW at one station, station 32, at the pole in the Amundsen Basin. One of the two stations that sampled in the Makarov Basin, station 38, had a bottom depth of 2,500 m and thus did not sample deep water masses. The remaining stations with water depth >1,000 m were in the Canada Basin or right above the Alpha Ridge and sampled CBDW (**Figure 1**).

RESULTS AND DISCUSSION FOR GN01

Shelf Waters of the Bering Strait and Chukchi Sea

Shallow bottom depths of ~50 m cause nutrient distributions in the Bering Strait and Chukchi Sea to be strongly influenced by interactions between processes in the water column and in bottom sediments. All stations in the Bering Strait and Chukchi Sea were ice – free during sampling. Isotope values were relatively uniform at stations 4 and 5 in the Bering Strait. $Si(OH)_4$ concentrations were relatively uniform with depth at station 4 but increased with depth at station 5. Stations 4 and 5 in the Bering Strait represent the Pacific end member with high silicic acid concentrations (20–40 $\mu mol\ kg^{-1}$) and $\delta^{30}Si(OH)_4$ values of +1.6 to +1.8‰; mean +1.72 ± 0.02‰ (n = 8) throughout the water column (**Figure 2**). Station 6 in the Chukchi Sea shows stronger surface (<20 m) silicic acid depletion and correspondingly elevated $\delta^{30}Si(OH)_4$ due to biological fractionation. Both silicic acid and isotope values at depths near the bottom at station 6 in the Chukchi Sea are more similar to those at stations 4 and 5 in the Bering Strait.

The other two stations in the Chukchi Sea, station 66 (35 m bottom depth) in the eastern region and station 61 at the Chukchi shelf break (72 m bottom depth), were sampled on the southward leg from the pole ~50 days after sampling stations 4, 5, and 6, allowing us to assess the impact of seasonal progression here. At station 66, silicic acid had been drawn down to <5 $\mu mol\ kg^{-1}$ throughout the water column and isotope values had increased to > + 3.0‰ (**Figure 2**). A strikingly different pattern was observed at station 61 at the shelf break where properties in the upper 20 m were similar to those at station 66, but silicic acid concentrations near the bottom (55–73 m) were as high as 58 $\mu mol\ kg^{-1}$ with isotope values of < + 1.5‰ (**Figure 2**). These are the highest silicic acid concentrations and lightest isotope values observed on GN01 (**Figure 3**); concentrations in the bottom 20 m are nearly twice those of any waters in the Chukchi Sea or in the Canada Basin suggesting that these unusual properties are not a transported signal. Near-bottom waters at station 61 also had the lowest value of N** observed on the cruise (−14.9 $\mu mol\ kg^{-1}$). N** is defined here as [0.87 × ([DIN] – 16 [$PO_4^=$] + 2.79)] where DIN is the sum of nitrate + nitrite concentrations. In the Chukchi Sea negative values of N** are diagnostic of sediment pore waters that have experienced denitrification and/or anammox (Aguilar-Islas et al., 2013). The extreme negative N** values near the bottom at station 61 are indicative of a likely benthic source for the observed high silicic acid concentrations and light isotope values consistent with GN01 observations of similar inferred benthic regeneration sources for both Cd and Zn in the Chukchi Sea (Jensen et al., 2019; Zhang et al., 2019).

Silicic acid derived from the dissolution of bSi from settled diatom frustules likely dominates the efflux although dissolution of mineral phases and metal oxyhydroxides may also contribute. Silicic acid derived from the dissolution of diatoms would be relatively light due to biological fractionation (De La Rocha et al., 1997) as would the Si from the dissolution of primary minerals (typical $\delta^{30}Si$ values <0‰, Frings et al., 2016) or oxyhydroxides, which are enriched in light isotopes of Si (Delstanche et al., 2009; Zheng et al., 2016). In contrast, processes such as authigenic clay formation (Opfergelt and Delmelle, 2012; Ehlert et al., 2016) and Si adsorption onto ferric hydroxides (Delstanche et al., 2009; Zheng et al., 2016) within sediments can preferentially remove lighter isotopes, increasing pore water $\delta^{30}Si(OH)_4$. Assuming that the near bottom waters at station 61 [58 $\mu mol\ kg^{-1}$ $Si(OH)_4$, $\delta^{30}Si(OH)_4$ = + 1.47‰] are a mixture of adjacent waters from similar depth [Station 57, 20 $\mu mol\ kg^{-1}$ $Si(OH)_4$, $\delta^{30}Si(OH)_4$ = + 1.75‰] with 58–20 = 38 $\mu mol\ kg^{-1}$ [$Si(OH)_4$] from pore waters, mass-balance yields an estimated isotopic composition of the pore water $Si(OH)_4$ of +1.32‰, similar to unpublished values for Barents Sea shelf pore waters (+1.16 ± 0.11‰, **Table 2**).

The Polar Mixed Layer of the Central Arctic Ocean

All stations located at latitudes <77.5°N were free of sea ice at the time of sampling (stations 52 through 61, **Figure 4**). The marginal ice zone (MIZ), the transition between open ocean and contiguous sea ice, was encountered between 77.5 and 79.0°N latitude (DiMento et al., 2019). Contiguous ice was present at all stations located north of 80°N in the Canada, Makarov, and Amundsen Basins (stations 30–46, ibid). Silicic acid concentrations in the PML of <5 $\mu mol\ kg^{-1}$ and $\delta^{30}Si(OH)_4$ > + 3.0‰ extended from the Chukchi Sea/Canada Basin shelf break, across the open water of the Canada Basin, through the MIZ and under the ice as far north as the Alpha Ridge at station 43 (85.1°N, **Figure 4**).

Surface waters north of 84°N latitude were part of the TPD as determined from the percent meteoric water derived by Charette et al. (2020) from salinity and $\delta^{18}O$ values according to Newton et al. (2013). Silicic acid concentrations in TPD waters were significantly higher compared to other PML waters and isotopically much heavier than other waters with similar [$Si(OH)_4$] (~10 $\mu mol\ kg^{-1}$, **Figure 3**). Those differences may arise from a combination of a strong river influence on Drift waters combined with active $Si(OH)_4$ consumption on shelves. Paffrath et al. (2021) note that in 2015 the TPD was heavily influenced by the Lena River and secondarily by the Yenisei and Ob Rivers based on dissolved neodymium isotopes and rare earth element concentrations. These rivers have high dissolved Si content (discharge-weighted average annual concentrations of 66, 93, and 81 $\mu mol\ kg^{-1}$ for the Lena, Ob, and Yenisei Rivers,

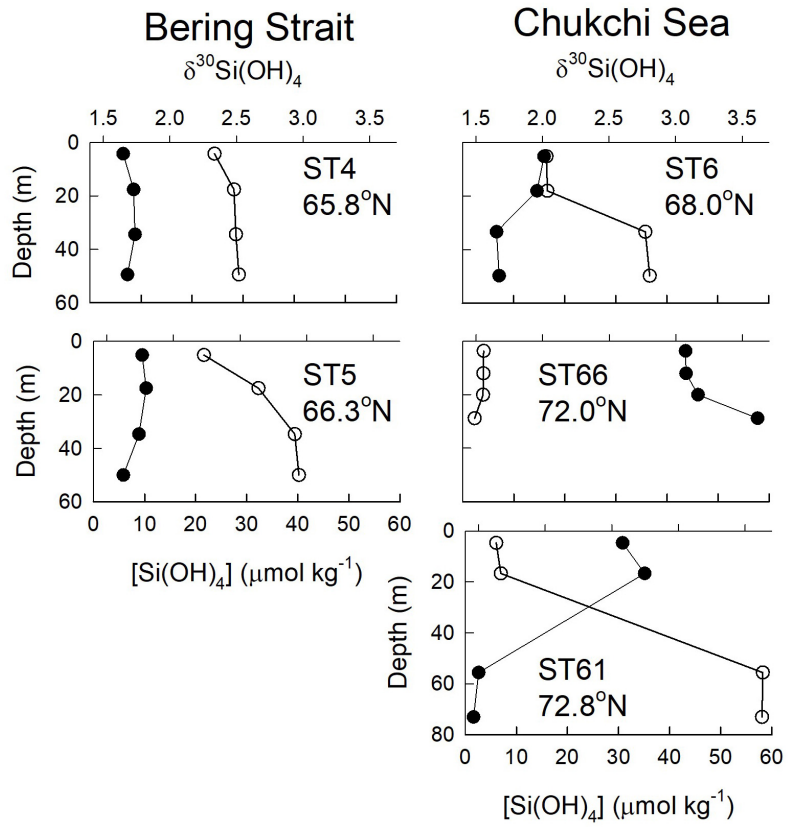

FIGURE 2 | Profiles of silicic acid concentration (open circles) and $\delta^{30}Si(OH)_4$ (filled circles) for stations in the Bering Sea (stations 4 and 5) and Chukchi Sea (Stations 6, 61, and 66).

respectively; Holmes et al., 2021) compared to Atlantic waters that have <10 μmol kg^{-1} (Torres-Valdés et al., 2013). Charette et al. (2020) estimate that $[Si(OH)_4]$ in the source waters feeding the TPD sampled during GN01 was 47 μmol kg^{-1} which would represent the net result of river inputs, benthic efflux, mixing, and biological consumption on the Eurasian shelf.

We are able to evaluate the influence of several of these sources on the $\delta^{30}Si(OH)_4$ of PML waters in the TPD. Sun et al. (2018) found the Si isotopic composition of the Lena River to vary seasonally from +1.17 ± 0.09‰ ($2\sigma_{SD}$) in autumn to +1.65 ± 0.09‰ ($2\sigma_{SD}$) in winter declining to values between +0.58 ± 0.09‰ ($2\sigma_{SD}$) and 1.04 ± 0.08‰ ($2\sigma_{SD}$) during peak spring flow that accounts for 60–80% of the annual discharge of Si (Holmes et al., 2012; Pokrovsky et al., 2013; Sun et al., 2018). Sun et al. (2018) estimate that the annual average $\delta^{30}Si(OH)_4$ for the major river input to the Arctic Ocean is +1.3 ± 0.03‰ (**Table 2**). Dissolved Si in sediment pore waters also tends to be isotopically light relative to overlying waters (Ehlert et al., 2016; **Table 2**) such that benthic efflux would also add light isotopes to shelf waters. The average $\delta^{30}Si(OH)_4$ of PML waters in the TPD of +2.29 ± 0.06‰ is heavy in comparison to both river and sediment inputs which, together with the relatively high $[Si(OH)_4]$ in the Drift, implies that Drift waters have evolved from water with initially high $[Si(OH)_4]$ that experienced considerable biological depletion and fractionation. This possibility is reinforced by the relationship between $\delta^{30}Si(OH)_4$ and the percent meteoric waters. A plot of $\delta^{30}Si(OH)_4$ versus% meteoric water content for all samples with >2% meteoric water contribution shows no clear pattern across all samples (**Figure 5A**); however, when data are separated by geographic location a linear relationship with a positive slope is seen in both the TPD and in the Canada Basin (**Figure 5A**) indicating that meteoric waters increase $\delta^{30}Si(OH)_4$ rather than leading to a decrease as would be expected from the input of unaltered river water.

The positive relationship between percent meteoric waters and $\delta^{30}Si(OH)_4$ in the PML of the Canada Basin has a steeper slope than in the TPD (**Figure 5A**). The Canadian Basin waters also have lower $[Si(OH)_4]$ (**Figure 5A**). This pattern could arise if freshwater source waters flowing into the Canada Basin have a heavier Si isotopic composition compared to those affecting PML waters in the TPD and/or if they become relatively more depleted and thus more highly fractionated in the Canada Basin than in the Drift. The Mackenzie River (**Figure 1**) dominates freshwater inflows into the Canada Basin (McClelland et al., 2012) although inputs from the Siberian shelves (Alkire et al., 2017) and the Yukon River via the Bering Strait also occur. The only Si isotope data from the Mackenzie River are from a single study conducted during summer (Pokrovsky et al., 2013).

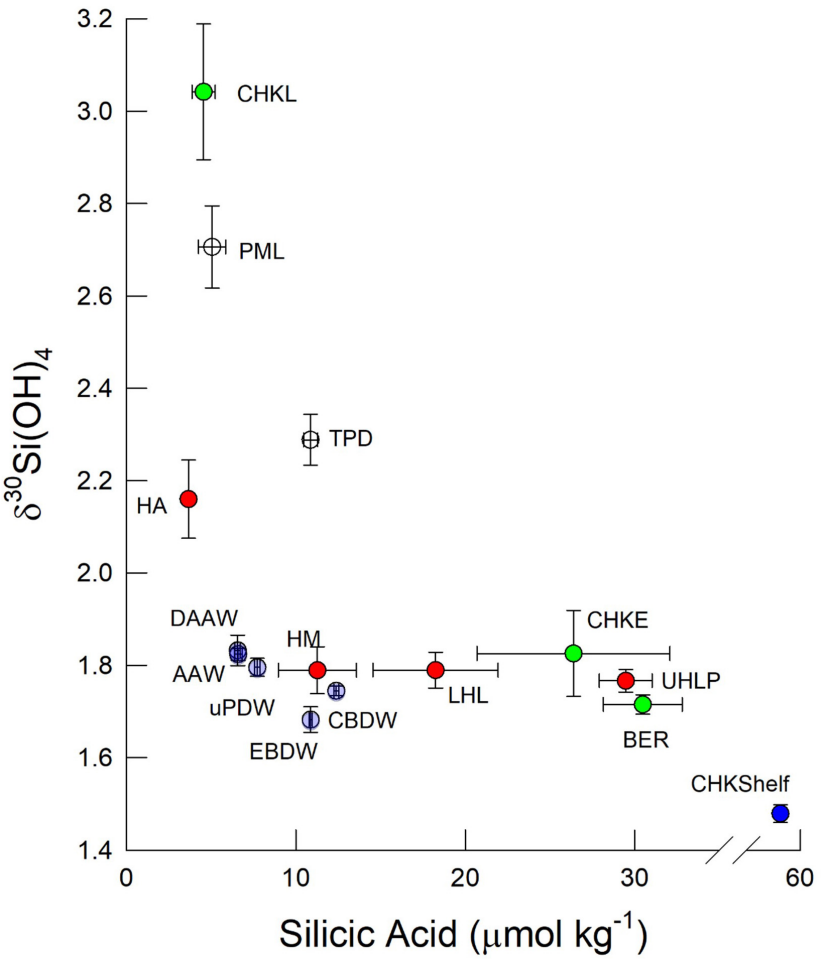

FIGURE 3 | Bivariate plot of $\delta^{30}Si(OH)_4$ and silicic aid concentration for water masses within the Arctic Ocean measured on GN01. Symbols represent means and uncertainty bars are one standard error of the mean. Color coding denotes water masses as follows: Green symbols denote data from the Bering Strait (BER) and Chukchi Sea (CHK) where samples from the Chukchi Sea are separated into those sampled early (CHKE) and late (CHKL). Blue symbols represent near bottom samples from the Chukchi Shelf break at station 61 (CHKShelf). White symbols are surface waters of the deep basins separated into the Polar Mixed Layer (PML) outside the Trans Polar Drift and PML waters within the Drift (TPD). Red symbols are halocline waters from the Amundsen Basin (HA), Makarov Basin (HM) and the upper and lower halocline of the Canada Basin, UHLP, and LHL, respectively, where the ULHP denotes UHL waters with >18 μmol kg^{-1} silicic acid. Light purple symbols denote intermediate waters as follows: Arctic Atlantic Waters (AAW) Deep AAW (DAAW) and upper Polar Deep Water (uPDW) and deep waters: Canada Basin Deep Water (CBDW) and Eurasian Basin Deep Water (EBDW).

The reported average $\delta^{30}Si$ of +1.36 ± 0.19‰ is comparable to values in Eurasian rivers on the Siberian Shelf from the same season, when $\delta^{30}Si$ values tend to be 0.5–1.0‰ higher than during peak flow (Pokrovsky et al., 2013; Sun et al., 2018; Paffrath et al., 2021). Those data suggest that differences in Si isotopic composition of the freshwater end members cannot explain the difference in slopes as the Mackenzie River appears to have a Si isotope composition similar to the Lena River that was the dominant influence on the TPD during GN01 (Paffrath et al., 2021). Dissolved Si concentrations also seem similar between the Mackenzie and Lena Rivers. Dissolved Si concentrations in the Mackenzie River average 50–60 μmol kg^{-1} (Emmerton et al., 2008) with a discharge-weighted average annual concentration of 56 μmol kg^{-1} (Holmes et al., 2021). The discharge-normalized annual average dissolved Si concentration for the Lena River (66 μmol kg^{-1}, Holmes et al., 2021) is only about 20% higher. The similarity of both the isotopic composition and the $[Si(OH)_4]$ of the Mackenzie and Lena Rivers combined with the lower $[Si(OH)_4]$ of waters with >2% meteoric water content in the Canada Basin (**Figure 5A**) suggest that the steeper slope of the relationship between meteoric water content and Si isotopic composition in the Canada Basin is driven by greater relative $Si(OH)_4$ depletion in the Canada Basin than in the TPD. The drivers of the implied difference in productivity are unclear, but may be related to a higher prevalence of open water in the Canada Basin versus more persistent contiguous ice in the TPD (**Figure 4**).

The trend of increasing $\delta^{30}Si(OH)_4$ with increasing percent meteoric waters observed in the Canada Basin and in the TPD on GN01 is opposite of the inverse relationship between

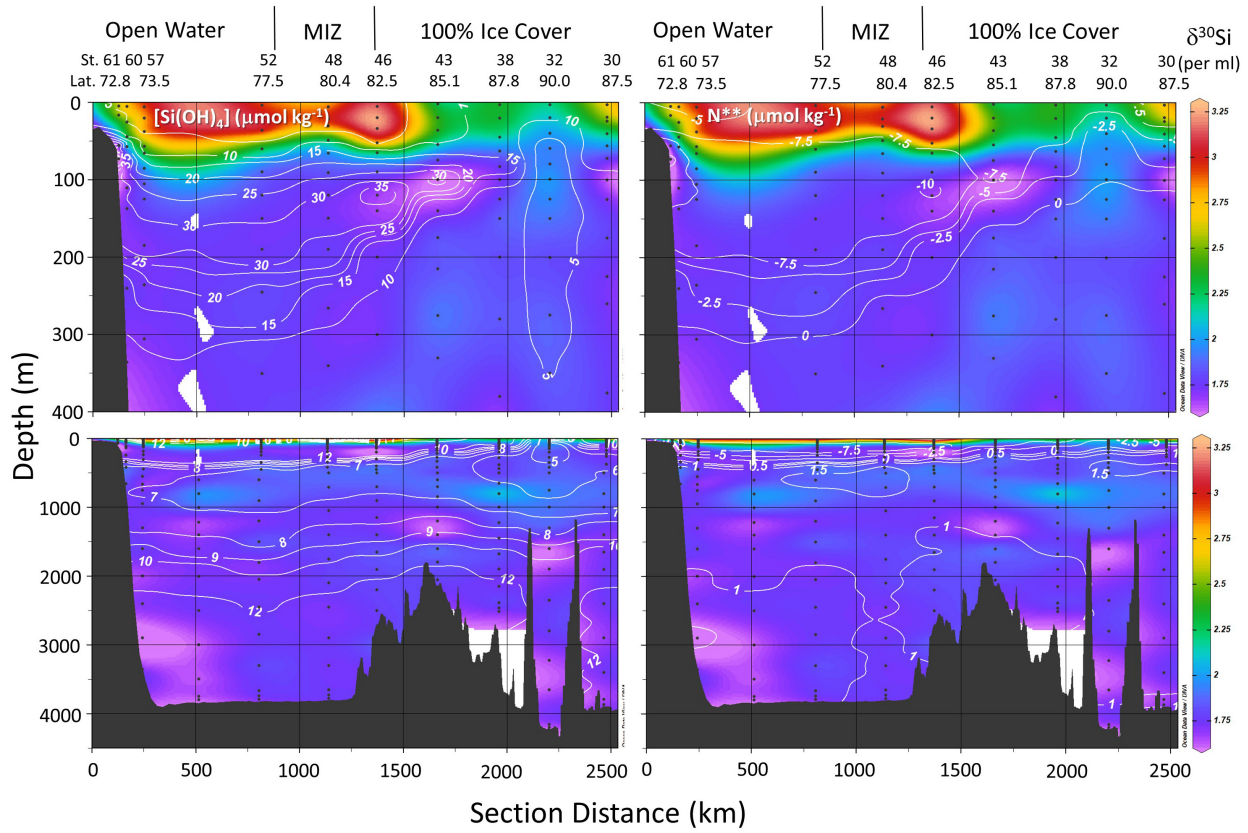

FIGURE 4 | Distribution of $\delta^{30}Si(OH)_4$ (color map) relative to line contours of silicic acid concentration in μmol kg^{-1} (left panels) and N** in μmol kg^{-1} (right panels) in the upper 400 m (top panels) and from surface to the sea floor (lower panels) on GN01 as a function of section distance. Section distance runs from station 61 in the Chukchi Sea to station 32 at the pole and then to station 32 in the Makarov basin (**Figure 1**) crossing the Lomonosov Ridge twice. Station numbers, station latitude, ice cover, and the location of the Marginal Ice Zone (MIZ) are indicated above each upper panel. Abbreviations denote the Canada Basin (CB), Makarov Basin (MB), and Amundsen Basin (AB). Bathymetric features include the Alpha Ridge (AR) and Lomonosov Ridge (LR).

these parameters in the Chukchi Sea (**Figure 5A**). An inverse relationship was also observed by Varela et al. (2016) in a section from the shelf offshore of the Mackenzie River to the central Canada Basin in August–September, 2009 (**Figure 1**). The reason for these differences is unclear. For GN01 the fractionation associated with the observed strong biological consumption of silicic acid (section "Shelf waters of the Bering Strait and Chukchi Sea") may have overwhelmed the influence of the modest levels of meteoric waters in the Chukchi Sea. For the Mackenzie River section, the shift in the relationship may be related to the known seasonal variability in Mackenzie River discharge or to changing diatom productivity on the shelf.

Values of $\delta^{30}Si(OH)_4$ were not related to the percent sea ice melt (%SIM) determined for GN01 by Charette et al. (2020) from salinity and $\delta^{18}O$ measurements (Newton et al., 2013). %SIM in the upper 500 m was negative under the contiguous ice from 80°N to the pole indicating the input of brine from sea ice formation rather than fresher water from ice melting. $\delta^{30}Si(OH)_4$ values show little relationship to %SIM over this depth range (**Figure 5B**). There is a weak positive relationship between $\delta^{30}Si(OH)_4$ and %SIM for samples within the PML (<65 m water depth, **Figure 5B**). Sea ice tends to be low in silicic acid (Tovar-Sánchez et al., 2010; Fripiat et al., 2017) reducing the impact of ice melt on upper water column $\delta^{30}Si(OH)_4$. Silicic acid in brine has a Si isotopic signature that is heavier than or nearly the same as the underlying seawater (Fripiat et al., 2007). The lower $\delta^{30}Si(OH)_4$ in waters with negative %SIM runs counter to this trend, suggesting that the correlation does not reflect a causal connection. The increasing $\delta^{30}Si(OH)_4$ with %SIM in the PML is also likely fortuitous with higher levels of productivity and silicic acid depletion in the more open waters within and south of the MIZ being the ultimate driver of the trend rather than any direct effect of ice melt.

Halocline Waters

The silicic acid maximum within the UHL (i.e., the UHLP, **Table 1**) extended from the Chukchi Shelf to the Alpha and Mendeleev Ridges separating the Canada and Makarov Basins (**Figure 4**). This maximum is often used to define the location of Pacific waters and reflects, in part, the high $[Si(OH)_4]$ of the Bering Strait inflow. The $Si(OH)_4$ maximum also tracks the depth horizon of a minimum in N** (**Figure 4**). As reinforced by our observations at station 61, low N** waters in the Chukchi Sea can

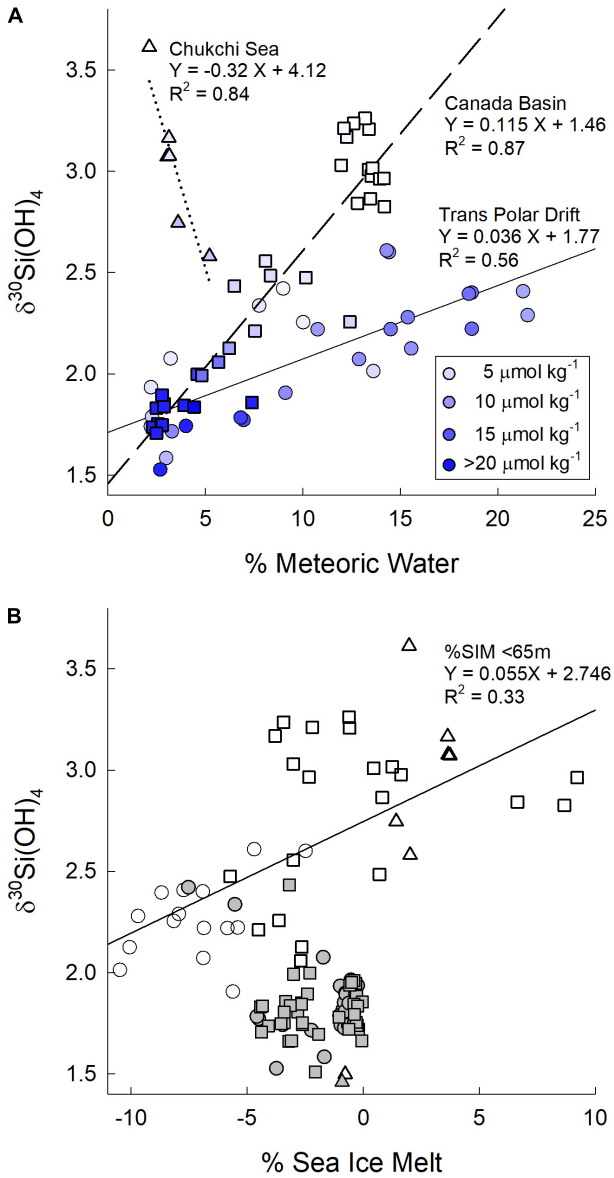

FIGURE 5 | (A) $\delta^{30}Si(OH)_4$ as a function of the % meteoric waters for surface waters in the transpolar drift (circles), the Canada Basin (squares), and in the Chukchi Sea (triangles). Shading of symbols is by silicic acid concentration as indicated in the legend. Solid, dashed, and dotted lines are linear regressions for the data in the transpolar drift, the Canada Basin and the Chukchi Sea, respectively. **(B)** $\delta^{30}Si(OH)_4$ as a function of the % sea ice melt for waters in the transpolar drift (circles), the Canada Basin (squares), and in the Chukchi Sea (triangles). Open symbols are for surface water <65 m. Filled symbols are for waters from 65 to 500 m.

indicate input of $Si(OH)_4$ from sediment pore waters (Aguilar-Islas et al., 2013) although the dissolution of resuspended from sediments may also play a role, as has been inferred for other biogeochemical processes in the region (Uchimiya et al., 2016; Xiang and Lam, 2020). The silicic acid concentrations and isotopic signature within the >18 µmol kg^{-1} $[Si(OH)_4]$ water of the UHLP falls between the averages for the Bering Strait and the early occupation station in the Chukchi Sea, reflecting contribution from both sources (**Figure 3**).

The pronounced maximum in $[Si(OH)_4]$ within the UHL has been shown to be associated with a minimum in $\delta^{30}Si(OH)_4$ (Varela et al., 2016). That minimum was not strong during GN01. Samples within the UHLP have a silicon isotope value of +1.77 ± 0.02‰ (n = 18) and an average $[Si(OH)_4]$ of 29.5 ± 1.6 µmol kg^{-1} compared to LHL waters of Atlantic origin with an average $\delta^{30}Si(OH)_4$ of +1.79 ± 0.05‰ (n = 5) and average $[Si(OH)_4]$ of 18.2 ± 3.7 µmol kg^{-1}. The higher UHLP would be expected to have a lower $\delta^{30}Si(OH)_4$ value given the general inverse relationship between dissolved Si concentration and Si isotope values in the sea (De La Rocha et al., 2000; Reynolds, 2009). Instead the UHL and LHL together form a broad minimum in $\delta^{30}Si(OH)_4$ between the heavier PML waters in the surface and the less pronounced subsurface maximum in $\delta^{30}Si(OH)_4$ that corresponds to AAW (**Figure 3**). The minimum is most pronounced at stations in the central Canada Basin (stations 46, 48, and 52; **Figure 6**).

The relative uniformity in $\delta^{30}Si(OH)_4$ across the UHL and LHL lies in sharp contrast to the large (>20 µmol kg^{-1}) range in $[Si(OH)_4]$ within the UHLP – LHL double halocline (**Figures 4**, **7**). This pattern could be explained by mixing between the LHL and underlying AAW as both the Si isotope signature and silicic acid concentration of LHL lies between those of the UHL and AAW (+1.82 ± 0.01‰, 6.6 ± 0.2 µmol kg^{-1}, **Figure 3**). Such mixing is evident when using Ga as a tracer of Pacific water in the Canada Basin (Whitmore et al., 2020) and has been invoked to explain the distribution of both dissolved Zn (Jensen et al., 2019) and DIC (Brown et al., 2016) in the halocline of the Canada Basin.

For the stations sampled for Si isotopes on GN01, the single halocline in the Makarov and Amundsen Basins lies below PML waters that are part of the TPD. Those halocline waters have meteoric water content of between 0.7 and 3%, suggesting some influence of the TPD drift in the halocline. In the Makarov Basin a peak in $[Si(OH)_4]$ and a minimum in $\delta^{30}Si(OH)_4$ occur just below the PML (**Figure 7**), suggesting penetration of Pacific waters into the Makarov Basin, although Alkire et al. (2019) argue that these waters formed on the East Siberian Shelf. In contrast, the opposite occurs in the Amundsen Basin where a minimum in $[Si(OH)_4]$ and maximum in $\delta^{30}Si(OH)_4$ are present at the depth where the percent contribution of meteoric waters first declines beneath the TPD (**Figure 7**).

Silicic acid concentrations in the halocline of both the Makarov and Amundsen Basins are half or less than those in the UHL and LHL of the Canada Basin, with the lowest average halocline concentration of 3.7 ± 0.2 µmol kg^{-1} observed in the Amundsen Basin (**Figures 3**, **7**). The average Si isotope composition of the halocline in the Makarov Basin is nearly identical to that in the LHL in the Canada Basin while it is heavier in the Amundsen Basin (**Figure 3**). The observation that the halocline in the Makarov Basin has the same isotopic signature as LHL in the Canada Basin, but lower $[Si(OH)_4]$, implies a lower concentration source water contributing to the halocline in the Makarov and/or one with a higher $\delta^{30}Si(OH)_4$ signal, consistent with a stronger influence of less modified Atlantic

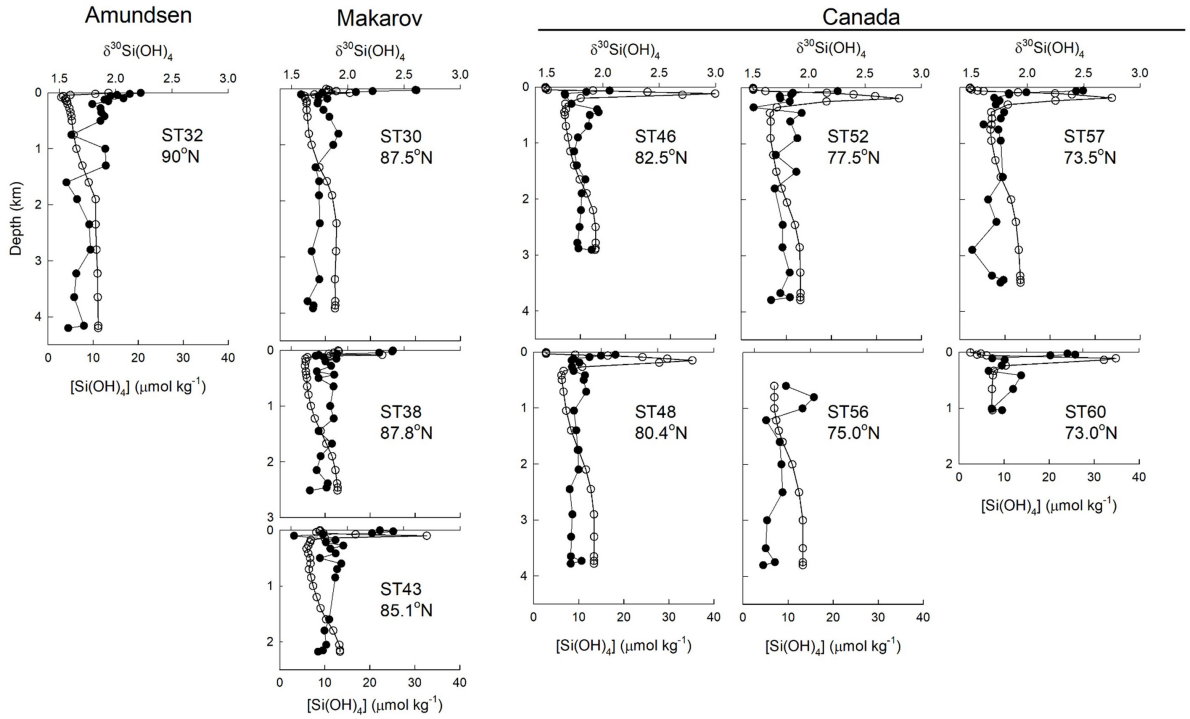

FIGURE 6 | Profiles of silicic acid concentration (open circles) and $\delta^{30}Si(OH)_4$ (filled circles) for stations in the Canada Basin (stations 46, 48, 52, 56, and 57), Makarov Basin (stations 30, 38), and Amundsen Basin (Station 32).

waters in the Makarov basin. The halocline in the Amundsen Basin is influenced by shelf and river waters from the Kara Sea (Paffrath et al., 2021). The heavy $\delta^{30}Si(OH)_4$ signature (+2.4‰) and low $[Si(OH)_4]$ (<4 μmol kg^{-1}) observed in the halocline of the Amundsen Basin (**Figure 7**) imply strong productivity leading to significant silicic acid depletion of such shelf waters prior to subduction.

Intermediate and Deep Waters

Overall, profiles of potential temperature, salinity and $[Si(OH)_4]$ from the base of the halocline (250 m) to near the sea floor cluster tightly for stations in the Canada Basin (**Figure 8**). Data from the two stations in the Makarov Basin generally track the properties observed in the Canada Basin, but contain slightly less $Si(OH)_4$ above 1,000 m and then again below 2,500 m (note that one station in the Makarov Basin has a bottom depth of 2,500 m, **Figure 8**). The one station in the Amundsen Basin is unique, with warmer saltier water and less $Si(OH)_4$ in the Atlantic layer than in the other two basins, and colder fresher bottom water that also has lower $Si(OH)_4$ (**Figure 8**).

The subsurface $\delta^{30}Si(OH)_4$ maximum in the warm saline AAW in the central Canada Basin was mentioned above. However, across all stations silicon isotopes in intermediate and deep waters show a general trend of a weak linear decrease $\delta^{30}Si(OH)_4$ with depth below the halocline, with no strong difference apparent among basins in the composite profile (**Figure 8**). The Atlantic water (both AAW and DAAW) and waters with uPDW characteristics lie above the ridge depths separating the three basins sampled. When samples from each water mass are averaged, AAW and DAAW show nearly identical average $[Si(OH)_4]$ and $\delta^{30}Si(OH)_4$ values (**Figure 3**). Isotope values decline and silicic acid concentrations increase in uPDW and these depth trends continue in both EBDW and CBDW (**Figure 3**). Although less $Si(OH)_4$-rich, EBDW has a slightly lower $\delta^{30}Si(OH)_4$ than does CBDW (**Figure 3**) which is statistically significant (*t*-test, $p = 0.04$; χ^2, $p = 0.001$).

SYNTHESIS

Comparison With Previous Data

Varela et al. (2016) report $[Si(OH)_4]$ and $\delta^{30}Si(OH)_4$ values along a section from the Mackenzie River across the shelf into the deep Canada Basin from the 2009 Canadian IPY-GEOTRACES expedition, ArcticNet 0903 (**Figure 1**). Offsets of 0.09–0.16‰ in $\delta^{30}Si(OH)_4$ are seen between isotope values measured for the same water mass from the present study and those of Varela et al. (2016) when using the definitions in **Table 1**. Such offsets have been reported before (Brzezinski and Jones, 2015; Liguori et al., 2020) and may arise in part from methodological and analytical differences between laboratories. In principle, the influence of these biases can be removed through normalization of each data set to seawater reference waters for Si isotopes (Grasse et al., 2017; see below). This approach cannot be applied to the data of Varela et al. (2016) as that study occurred before reference seawaters for Si isotopes were available. Instead the ArcticNet 0903 and GN01

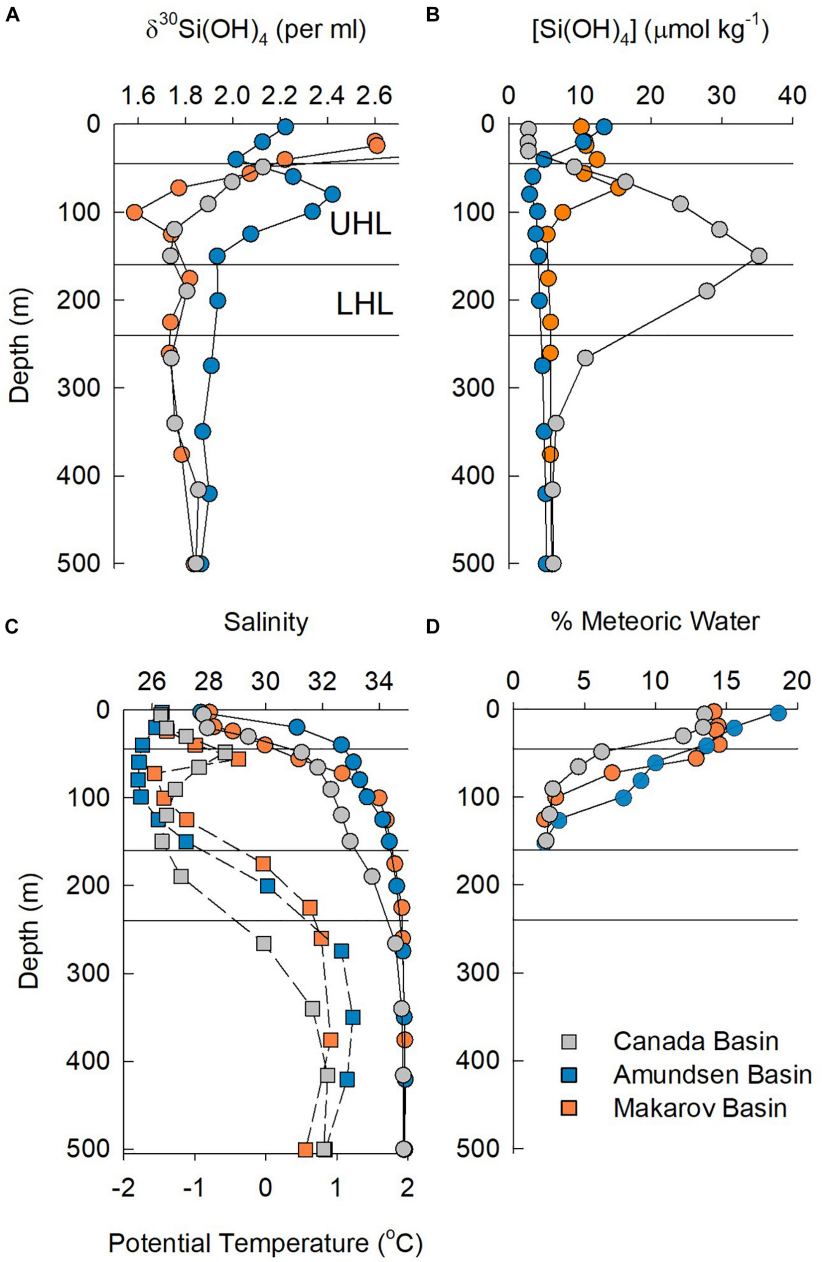

FIGURE 7 | Properties in the upper 500 m at station 48 in the Canada Basin, station 30 in the Makarov Basin, and station 32 in the Amundsen Basin. **(A)** Silicon isotope values, **(B)** silicic acid concentration, **(C)** salinity (squares) and potential temperature (circles), and **(D)** % meteoric waters. Horizontal lines denote the approximate boundaries of the UHL and LHL.

datasets were normalized using results from intercalibration stations by first determining the average difference in Si isotope values for samples from common depths in deep waters between 2,700 and 3,000 m where temporal changes should be minimal. The average offset (ArcticNet 0903 minus GN01) of -0.11 ± 0.04 ‰ (always $\pm$ 1σ_{SE}) was then applied to Si isotope samples from all depths in the ArcticNet 0903 data set.

The minimum in $\delta^{30}Si(OH)_4$ associated with Pacific waters within the halocline of the Canada Basin is similar in both data sets. The adjusted UHLP average $\delta^{30}Si(OH)_4$ for ArcticNet 0903, $+1.71 \pm 0.05$‰ ($n = 10$), $[Si(OH)_4]$ of 27.4 ± 1.4 μmol kg^{-1}, and the adjusted LHL average of $+1.72 \pm 0.05$‰ ($n = 7$), $[Si(OH)_4]$ of 19.0 ± 4.0 μmol kg^{-1}, are both within 0.07‰ of GN01 values for the same features. The major difference is in the underlying AAW that is on average 0.16 ± 0.06‰ ($n = 16$) heavier in the adjusted ArcticNet 0903 data set than observed on GN01. Upon closer examination, that difference is driven by an onshore-offshore gradient in the adjusted $\delta^{30}Si(OH)_4$ signature of AAW in the

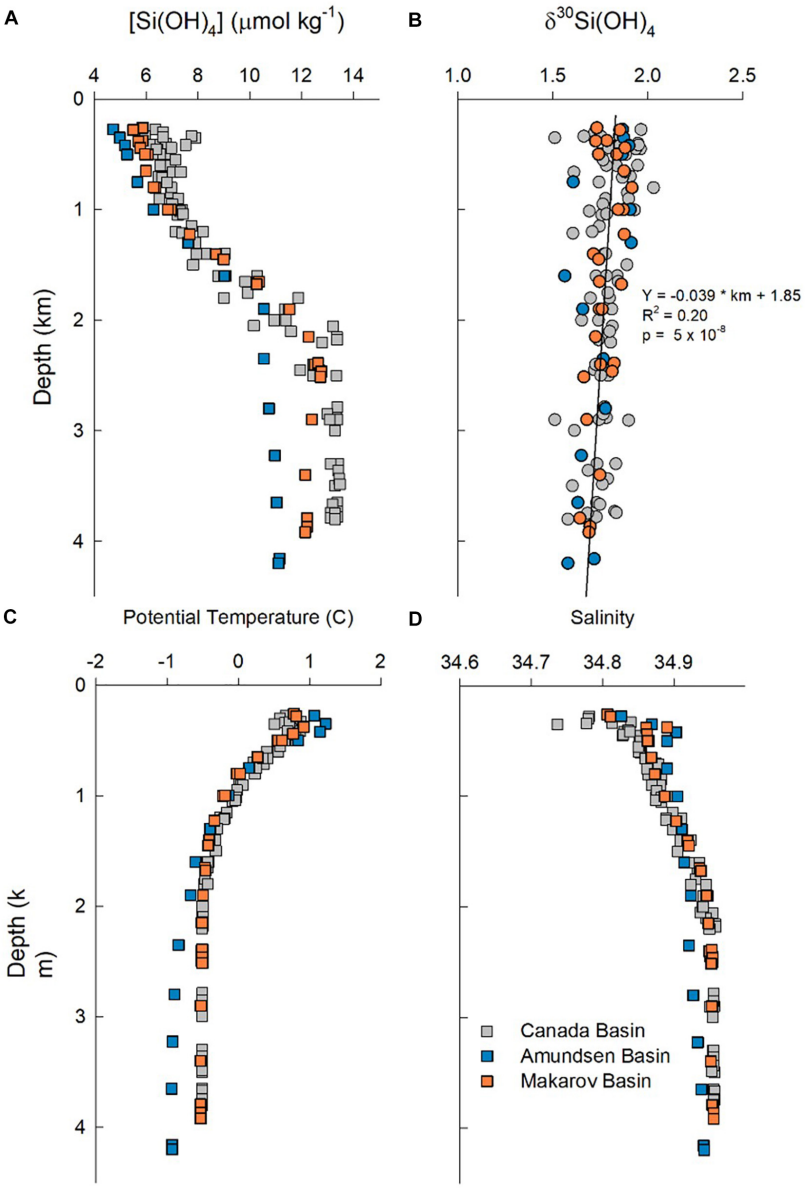

FIGURE 8 | Profiles of water column properties below 250 m. **(A)** Silicic acid concentration, **(B)** $\delta^{30}Si(OH)_4$, **(C)** potential temperature, and **(D)** salinity. Colors denote stations in the Canada Basin (gray symbols), Makarov Basin (orange symbols), and the Amundsen Basin (blue symbols).

ArcticNet 0903 data set from +2.02 ± 0.04‰ (n = 6) at station L1.1 closest the coast, to +1.97 ± 0.05‰ (n = 4) at station L2, to +1.82 ± 0.06‰ (n = 4) at station L3 furthest offshore in the Canada Basin in 3,000 m water depth (**Figure 1**). The value at station L3 matches the average $\delta^{30}Si(OH)_4$ for AAW on GN01 at stations 46, 48, and 52 (mean = + 1.84 ± 0.03‰, n = 10) which are also located in the central Canada basin where water depth exceeds 3,000 m. The offshore gradient in the isotopic composition of AAW may be related to circulation. The gradient occurs in a region where Atlantic waters from the FSB (AAW) flow from the west to the east after having crossed the Eurasian Shelf and Chukchi Sea Borderlands (Li et al., 2020 and references therein, **Figure 1**). The flow is concentrated in two jets that follow the 1,000–1,500 and 2,500–3,000 m isobaths, with both jets displaying significant interannual variability in alongshore velocity (Li et al., 2020).

In addition to complementing the ArcticNet 0903 data set, the GN01 data adds to silicon isotope measurements in the Bering Strait and Chukchi Sea during the Canadian Distributed Biological Observatory program cruise DBO15 (Giesbrecht, 2019), during GEOTRACES GN03 in the Canada Basin (Giesbrecht, 2019) and during GEOTRACES GN04 in the Makarov, Amundsen, and Nansen Basins (Liguori et al., 2020; **Figure 1**). Together data from DBO15, GN01, GN03, and GN04

allow a more thorough assessment of the isotopic composition of key water masses. To standardize the data from each expedition, given evidence for inter-laboratory offsets (section "Crossover Stations and Intercalibration"), we take advantage of the values reported in each study for the Si isotope reference seawater $ALOHA_{1,000}$. Both the present study, Giesbrecht (2019) and Liguori et al. (2020) report the average value for this material from analyses conducted alongside the analysis of seawater samples from GN01, GN03, DBO15, and GN04. Here we use the difference between the average $\delta^{30}Si(OH)_4$ value for $ALOHA_{1,000}$ obtained by each laboratory and the consensus value for $ALOHA_{1,000}$ of +1.24 ± 0.03‰, n = 11 (Grasse et al., 2017) to normalize each data set to this value, leading to adjustments of −0.05 ± 0.03‰ for $\delta^{30}Si(OH)_4$ values from GN01, −0.05 ± 0.05‰ for those from GN03 and DBO15 and of +0.07 ± 0.11‰ for values from GN04.

Giesbrecht (2019) found conditions in the Bering Strait and Chukchi Sea in July 2015 (DBO15) that were very similar to those observed during GN01 in September of the same year. $ALOHA_{1,000}$ – adjusted $\delta^{30}Si(OH)_4$ values for stations from the Bering Strait on DBO15 averaged +1.76 ± 0.05‰ with $[Si(OH)_4]$ of 31.0 ± 1.6 μmol kg^{-1} compared to +1.67 ± 0.04‰ and $[Si(OH)_4]$ of 30.5 ± 2.3 μmol kg^{-1} on GN01. In the Chukchi Sea, very similar $Si(OH)_4$ concentrations were observed at stations sampled on DBO15 and those sampled in September on GN01 (26.9 ± 3.7 and 26.4 ± 5.7 μmol kg^{-1} for DBO15 and GN01, respectively), although adjusted isotope values were higher on DBO15 (+2.18 ± 0.12‰) compared to GN01 (+1.78 ± 0.10‰), possibly reflecting the variability in the balance between silicic acid regeneration, consumption and benthic influence in this highly productive and shallow region. This variability is also consistent with the differences observed during GN01 when comparing stations from the Chukchi Sea sampled 50 days apart (section "Shelf Waters of the Bering Strait and Chukchi Sea").

Comparisons within the central Arctic Ocean are restricted to the halocline and greater depths as GN03 did not sample the upper 50 m and the data reported for GN04 by Liguori et al. (2020) are all from depths >∼200 m. The minimum in adjusted $\delta^{30}Si(OH)_4$ values within the >18 μmol kg^{-1} silicic acid waters of the UHLP in the Canada Basin was somewhat more intense on DBO15/GN03 (+1.60 ± 0.06‰) than on GN01 (+1.72 ± 0.04‰) despite similar average silicic acid concentrations (29.4 ± 3.1 versus 29.5 ± 1.5 μmol kg^{-1} on GN03 and GN01, respectively). The difference likely reflects the variability resulting from coarse resolution spatial sampling across very strong depth gradients (**Figure 4**) and the effect of small sample size (n = 4) for UHLP waters for the DBO15 data set compared to that for GN01 (n = 15).

The adjusted data for GN01, GN03, DBO15, and GN04 show the same systematic trends among intermediate and deep water masses (**Table 3**). The data from each cruise was subdivided based on the water mass definitions in **Table 1**, and thus the reported values differ slightly from the end member estimates presented by Liguori et al. (2020) for GN04 and by Giesbrecht (2019) for GN03 and DBO15 that used slightly different definitions. The AW found in the Eurasian basin during GN04 has a $\delta^{30}Si(OH)_4$ value slightly lighter than AAW in the Amerasian Basin. Along its cyclonic flow path around the Arctic Ocean (Aksenov et al., 2011), AW cools and freshens through sea ice interactions on the shelves, transforming into AAW (Schauer et al., 1997; Rudels et al., 2005; Rudels, 2012). Silicic acid concentrations increase in AAW relative to AW, possibly reflecting the inputs of dissolved Si from shelf sediments and rivers. However, those sources all have $\delta^{30}Si(OH)_4$ values lower than that of AW and thus the increase in $\delta^{30}Si(OH)_4$ between AW and AAW (**Table 3**) likely arises through fractionation during partial biological consumption of the silicic acid added to the water mass on shelves (see section "The Polar Mixed Layer of the Central Arctic Ocean").

The adjusted isotopic signature of DAAW is the same as that of AAW while $[Si(OH)_4]$ is slightly lower (**Table 3**). The decline in $[Si(OH)_4]$ is mainly due to the differences in concentrations in the water mass between the Eurasian and Amerasian Basins (**Table 3**), suggesting that DAAW gains silicic acid during advection. From DAAW to greater depths $\delta^{30}Si(OH)_4$ progressively declines and $[Si(OH)_4]$ progressively increases (**Figure 8** and **Table 3**). Both EBDW and CBDW are isotopically lighter than overlying intermediate waters with EBDW being the lightest and slightly lower in $Si(OH)_4$ relative to CBDW on both GN01 and GN04. The isotopic difference is statistically significant for data from GN01, but not for GN04 (Liguori et al., 2020). However, given the consistency of the pattern between studies, the decrease in $\delta^{30}Si(OH)_4$ between CBDW and EBDW is likely robust.

The adjusted deep water values for CBDW and EBDW are both lighter than the value of +1.88 ± 0.12‰ reported for CBDW by Varela et al. (2016) by about 0.2‰ (see discussion above). Nonetheless, the adjusted $\delta^{30}Si(OH)_4$ of deep waters observed during both GN01 and GN04 are considerably heavier than the +1.2 to +1.4‰ values typical of other deep ocean basins (Cardinal et al., 2005; Reynolds et al., 2006; Beucher et al., 2011; de Souza et al., 2012b) and thus support the conclusion of Varela et al. (2016) that the Arctic Ocean contains the heaviest deep waters in the global ocean. To further assess the mechanisms leading to the heavy isotopic signature of the deep Arctic the Si budget of the Arctic Ocean is examined below, in order to identify the major processes that impact isotope dynamics.

Arctic Ocean Silicon Budget

Silicon budgets for the Arctic Ocean extend back to the 1970s (Codispoti and Lowman, 1973; Codispoti and Owens, 1975). Most assessments indicate that the major marine Si inflows and outflows in the Arctic Ocean are in balance (Jones and Coote, 1980; Anderson et al., 1983) or nearly balanced (Torres-Valdés et al., 2013). The most recent analysis by Torres-Valdés et al. (2013) examined Si fluxes across the major Arctic gateways of the Bering Strait, Davis Strait, Fram Strait, and Barents Sea (**Figure 1**) and concluded that the Arctic Ocean is a slight net exporter of $Si(OH)_4$. Here the silicic acid budget of Torres-Valdés et al. (2013) is used to inform a first-order Si isotope budget.

Table 2 shows the Torres-Valdés et al. (2013) $Si(OH)_4$ budget together with estimates of other inputs and outputs of Si derived from the literature. Silicic acid inputs through the major marine Arctic gateways are dominated by inputs from the Pacific Ocean through the Bering Strait and from the Atlantic Ocean over the Barents Sea shelf, with the contribution of the Pacific water

TABLE 2 | Silicic acid and Si isotope budget for the Arctic Ocean.

Gateway	Tmol Si a^{-1} [a]	$\delta^{30}Si(OH)_4$ (‰) [b]	Isotope data source
Davis Strait	−1.35 ± 0.16	+1.75 ± 0.07	Giesbrecht, 2019[f]
Fram Strait	−0.22 ± 0.19		
Input		+1.74[e]	Liguori et al., 2020
Output		+1.79 ± 0.09	This study, **Table 5**
Barents Sea	0.42 ± 0.07		
Bering Strait	0.66 ± 0.08	+1.67 ± 0.04	This study
		+1.76 ± 0.05	Giesbrecht, 2019
Total	−0.50 ± 0.20		
Additional inputs			
River discharge dissolved Si	0.41	+1.3 ± 0.3	Sun et al., 2018
River discharge Biogenic Silica	0.02–0.08[k]		
Additional outputs			
Opal burial	−0.16[l]	+1.16 ± 0.10[g]	Liguori et al., 2020
	−0.30[l]		
Total[i]	−0.14 – −0.35		
DSOW		+1.56 ± 0.28[h]	
ISOW		+1.60 ± 0.07[h]	
LSW		+1.68 ± 0.10[h]	
Internal cycling			
Net silica production	3.6[d]		
Gross silica production	7.2[j]		
Benthic efflux	0.39[c]	+1.16 ± 0.11[m]	Ward and Hendry, pers. comm.

[a] *Inputs and outputs through Gateways and river discharge of dissolved Si from Torres-Valdés et al. (2013).*
[b] *Seawater $\delta^{30}Si(OH)_4$ normalized using deviations from $ALOHA_{1,000}$ consensus value. Errors are standard errors.*
[c] *Midpoint of range of 0.35 to 0.42 Tmol Si a^{-1} given by März et al. (2015).*
[d] *MacDonald et al. (2010).*
[e] *Atlantic water inflow through Fram Strait.*
[f] *$\delta^{30}Si(OH)_4$ in Canadian Archipelago, +1.77 ± 0.07‰ reported by Giesbrecht (2019).*
[g] *Average $\delta^{30}Si(OH)_4$ of biogenic silica in the water column at depths >500 m (Liguori et al., 2020).*
[h] *$ALOHA_{1,000}$ adjusted values from Sutton et al. (2018) and de Souza et al. (2012b).*
[i] *Assumes half of the biogenic silica entering from rivers dissolves (Tréguer et al., 2021).*
[j] *Assumes a silica dissolution:production ratio of 0.50 (Tréguer and De La Rocha, 2013).*
[k] *Carey et al. (2020).*
[l] *0.16 Tmol Si a^{-1} from main text; 0.30 Tmol Si a^{-1} estimate from MacDonald et al. (2010).*
[m] *Average of pore water measurements (0–0.5 cm) from nine cores collected from three sites in each of 3 years.*

entering through the Bering Strait being about 60% larger. Dominant outflows are through the Davis Strait that drains the Canadian Archipelago followed by the East Greenland current in the Fram Strait. Inflows (1.08 Tmol Si a^{-1}) are less than outflows (1.57 Tmol Si a^{-1}), leading to a net outflow of about 0.5 Tmol Si a^{-1} to the North Atlantic.

One Si removal term that has not been part of past Si budgets for the Arctic Ocean is opal burial. Arctic sediments are opal poor, with generally <5% opal (März et al., 2015). Early estimates of sediment accumulation rates of a few mm ka^{-1} implied negligible opal burial in the Arctic Ocean (Backman et al., 2004); however, revised age models increased accumulation rates to 1–3 cm ka^{-1} (ibid). Assuming an average sedimentation rate of 2 cm ka^{-1}, an average opal content of 2% and a bulk density of 1.70 g cm^{-3} (ibid) across the Arctic seabed (**Table 4**) yields an estimate of the annual opal burial rate of 0.16 Tmol Si a^{-1} (**Table 2**). A second estimate is obtained by applying the same opal content of 2% to the total bulk sediment burial rate for the Arctic Ocean of 1,008 Mt a^{-1} (MacDonald et al., 2010), yielding an opal burial of 0.30 Tmol Si a^{-1} (**Table 2**). Thus, burial plus outflows lead to an annual net removal of 0.66–0.80 Tmol Si a^{-1} from the Arctic Ocean.

River inputs of dissolved Si have a stronger influence in the Arctic compared to the rest of the global ocean. The global ocean outside of the Arctic receives about 5.4 Tmol Si a^{-1} of dissolved Si from rivers, compared to a total global ocean inventory of Si of 120,000 Tmol (Tréguer et al., 2021). By comparison, river inputs of dissolved Si to the Arctic have been estimated to be 0.41 Tmol Si a^{-1} (**Table 2**) against an estimated inventory of 196 Tmol (**Table 4**). Thus, the impact from rivers on the Si budget is 50 times greater in the Arctic Ocean than in the ocean as a whole.

In addition to dissolved silicon, Arctic rivers discharge 0.02–0.08 Tmol Si a^{-1} as particulate bSi into the Arctic Ocean (Carey et al., 2020; **Table 2**). Assuming that about half of that material dissolves before burial (Tréguer et al., 2021), the total riverine input offsets about 53–68% of the estimated net removal of Si from the Arctic Ocean. Additional inputs of Si from hydrothermal vents occur along the Gakkel Ridge (Edmonds et al., 2003; Liguori et al., 2020), but the magnitude of that influx is currently unknown. Given present uncertainties it is difficult

TABLE 3 | Average silicon isotope values in per mil and silicic acid concentration in μmol kg^{-1} for major water masses as defined in **Table 1**.

Cruise	Water mass					
	AW[a]	AAW	DAAW	uPDW	EBDW	CBDW
GN01						
$\delta^{30}Si(OH)_4$		+1.78 ± 0.03	+1.78 ± 0.05	+1.75 ± 0.04	+1.63 ± 0.04	+1.70 ± 0.03
$[Si(OH)_4]$		6.59 ± 0.23	6.56 ± 0.16	7.72 ± 0.16	10.87 ± 0.10	12.38 ± 0.16
n		37	12	21	7	53
GN03						
$\delta^{30}Si(OH)_4$		+1.79 ± 0.12[c]	+1.76 ± 0.09	+1.76 ± 0.15		+1.66 ± 0.07
$[Si(OH)_4]$		7.46 ± 0.24	7.66 ± 0.25	8.91 ± 0.26		12.31 ± 0.41
n		2	3	4		6
GN04						
$\delta^{30}Si(OH)_4$	+1.58 ± 0.73		+1.69 ± 0.11	+1.60 ± 0.11	+1.52 ± 0.11	+1.55 ± 0.12
$[Si(OH)_4]$	4.84 ± 0.13		5.62 ± 0.09	8.79 ± 0.42	11.51 ± 0.07	12.49 ± 0.12
n	3		21	12	25	7
Averages[b]						
$\delta^{30}Si(OH)_4$	+1.58 ± 0.73	+1.78 ± 0.03	+1.76 ± 0.04	+1.73 ± 0.04	+1.62 ± 0.04	+1.69 ± 0.03
$[Si(OH)_4]$	4.84 ± 0.13	7.01 ± 0.16	6.01 ± 0.08	8.12 ± 0.13	11.30 ± 0.06	12.44 ± 0.09

Isotope values are normalized using deviations from ALOHA$_{1,000}$ consensus value. Uncertainty terms are one standard error of the means and include error propagation of the normalization to ALOHA$_{1,000}$ consensus value. N refers to the number of unique seawater samples averaged.
[a] *Differs from value in **Table 1** which is the estimate for 100% AW based on the OMPA of Liguori et al. (2020).*
[b] *Weighted averages and weighted errors of the cruise means (e.g., Leo, 1994).*
[c] *Calculated using data from stations CB3 and CB4 in the deep central basin. Excludes station CB2 close to the shelf break.*

TABLE 4 | Silicic acid inventory of the Arctic Ocean.

	Surface area (m^2) × 10^{13}	Volume (m^3) × 10^{16}	$[Si(OH)_4]$ (μmol Si kg^{-1})	$[Si(OH)_4]$ (Tmol)
Entire basin	1.5558[a]	1.875[a]		
Upper 150 m (Shelves)		0.233	10[b]	23
150–2,000 m		0.821	9[c]	75
>2,000 m		0.821	12[c]	99
Total				196

[a] *Eakins and Sharman (2010).*
[b] *Accounts for high silicic acid from Pacific and river inputs.*
[c] *Average value from GN01 and GN04 over this depth range.*

to close the silica budget for the Arctic Ocean, but potential imbalances are not large in absolute terms (**Table 2**).

Inspection of **Table 2** shows that internal Si cycling within the Arctic Ocean is dominated by the production and dissolution of bSi. Annual net silica production for the Arctic Ocean has been estimated to be 3.6 Tmol Si a^{-1} based on extrapolations of annual net primary productivity and new production (MacDonald et al., 2010). Gross silica production is higher due to losses of silica to dissolution in the euphotic zone. The only measures of silica dissolution:production (D:P) ratios from the euphotic zone of the Arctic Ocean are for the Bering and Chukchi Seas under post-bloom conditions (Giesbrecht, 2019). Those ratios exceeded unity, indicating no potential for silica export to sediments at that time. Such high values for a post-bloom scenario are not surprising as D:P ratios typically increase after blooms (Brzezinski et al., 2003; Beucher et al., 2004). Seasonal information on D:P values from the Southern Ocean (Brzezinski et al., 2001; Beucher et al., 2004; Closset et al., 2014) suggest that, on average, gross silica production in polar waters is about twice net silica production (Tréguer and De La Rocha, 2013). Applying that average to the Arctic Ocean results in an estimated gross silica production of 7.2 Tmol Si a^{-1}. That value exceeds all individual abiotic fluxes, including opal burial, by nearly an order of magnitude. Even if only approximately correct, this level of gross silica production makes biological uptake and opal recycling important, if not the dominant, processes in the Si budget for the Arctic Ocean, in agreement with the conclusion of a strong biological influence on Al and Si cycling in the Arctic Ocean by Middag et al. (2009). Large biological fluxes create the potential for the reorganization of Si beyond water-mass mixing, since such high internal biological fluxes imply that opal burial, which is small in relative terms compared to opal production, can still be significant in comparison to the other fluxes associated with the Arctic Si budget. This is particularly true on Arctic shelves where opal production is highest, opal export is highest and most seasonal (MacDonald et al., 2010), and therefore a significant fraction of Si recycling gets shifted toward the seafloor.

The opal burial flux estimated above, 0.16–0.30 Tmol Si a^{-1}, equals 2–4% of the estimated surface gross silica production, which compares well with the global average of 3% (Tréguer et al., 2021) and implies that 96–98% of gross silica production in the Arctic Ocean is lost to dissolution. The assumed D:P ratio above presumes that half is lost in the euphotic zone. The estimated sediment efflux of 0.39 Tmol Si a^{-1} (März et al., 2015) indicates that 5% of gross silica production dissolves and is released from sediments, leaving the remaining 45% to dissolve in the water column between the base of the euphotic zone and the sea floor. Thus, on Arctic-Ocean average, dissolution within the water column is the overwhelmingly dominant term in silica recycling, accounting for 50% + 45% = 95% of total silicic acid regeneration. Like the other biologically mediated fluxes this ocean-wide estimate averages across significant regional variability especially the contrasting dynamics on shelves versus the deep basins (see section "Preliminary Arctic Ocean Silicon Isotope Budget"). While subject to significant uncertainty the estimate points to the first-order importance of biological fluxes in the Arctic Ocean.

Assuming steady state, the average whole-ocean residence time of Si in the Arctic Ocean equals the total Si inventory in the basin divided by total inputs (or outputs). We estimate the total inventory of $Si(OH)_4$ in the Arctic Ocean to be 196 Tmol Si (**Table 4**), which is likely only good to within 20%. Given that inflows and outflows are nearly balanced, we use the outflow determined by Torres-Valdés et al. (2013) of 1.57 Tmol Si a^{-1} (**Table 2**) to calculate an average residence time of 125 years. That value averages across the years- to decades- long residence time of the PML and halocline (Ekwurzel et al., 2001) and the centuries-long residence times of deep waters (Timmermans et al., 2003; Tanhua et al., 2009). The biological residence time of (196 ÷ 7.28, i.e., total inventory divided by gross silica production) 27 years is far shorter than the whole-ocean residence time implying that each molecule of Si in the Arctic Ocean passes through a diatom five times before burial in the sediments or transport out of the Arctic Ocean. The implied level of biological influence on the Arctic Ocean Si cycle is less than for the global ocean where it is estimated that an atom of Si entering the sea passes through a diatom 17 times before burial in the seabed (Tréguer et al., 2021). The implications of a weaker biological influence in the Arctic compared to the rest of the global ocean for Si isotope dynamics are discussed at the end of section "Preliminary Arctic Ocean Silicon Isotope Budget."

Preliminary Arctic Ocean Silicon Isotope Budget

Sufficient $\delta^{30}Si(OH)_4$ data now exist to address some key aspects of the Arctic Ocean Si isotope budget. Direct measurements are presently available for the inflow though the Bering Strait and the outflow through the Davis Strait (**Table 2**). Isotopic data for inflow over the Barents Sea shelf and exchange through the Fram Strait are currently lacking; however, Liguori et al. (2020) provide an estimate of the isotopic composition of the AW inflow through the Fram Strait based on their water mass analysis (**Table 2**). A preliminary estimate of the isotopic composition of outflows through the Fram Strait was calculated by combining the $\delta^{30}Si(OH)_4$ and $[Si(OH)_4]$ in key water masses (**Tables 2**, **5**) with the annual transport of each water mass through the Strait (Marnela et al., 2016). A similar calculation for Barents Sea inflows was not possible due to the lack of estimates of the isotopic composition of end members. Note that all values in **Table 2** have been normalized to the $ALOHA_{1,000}$ reference seawater as described in section "Comparison With Previous Data."

What is striking about the partial isotope budget is the similarity of the isotopic values of inflows compared to outflows across the major Arctic Ocean gateways (average values range from +1.71 to +1.77‰, **Table 2**). The heavy nature of inflows supports the postulate of Varela et al. (2016) that the heavy isotopic signature of inflows to the Arctic Ocean contribute to the overall heavy Si isotopic signature of deep waters within the Canada Basin, and by extension, the other deep Arctic Ocean basins. Varela et al. (2016) based their hypothesis on the shallow sills separating the Arctic Ocean from the Pacific and Atlantic Oceans and the observation that $\delta^{30}Si(OH)_4$ generally increases from depth to the surface in the upper 2 km of other ocean basins. Si isotope data for Arctic Ocean inflows and outflows were not available at that time. The data summary presented here confirms their idea for two of the three major inflows. Moreover, the similarity among inflows and outflows illustrated in **Table 2** also implies only subtle net alteration of the primary inflowing isotope signature by internal processes within the Arctic Ocean.

The similarity in the isotopic composition of the silicic acid entering and leaving the Arctic Ocean is surprising, as dynamics within the Arctic Ocean are known to play a major role in redistributing Si isotopes among the major Arctic water masses (Liguori et al., 2020). The major processes within the Arctic Ocean that can alter the Si isotope signature of waters masses include mixing, river inputs of dissolved and particulate Si, biological uptake and the dissolution and burial of bSi. Alterations due to water mass mixing and internal dynamics reported earlier (Liguori et al., 2020), and confirmed here, do set up a depth gradient in $\delta^{30}Si(OH)_4$. Below the halocline, major water masses become progressively isotopically lighter to the extent that deep waters, where about half of the silicic acid in the Arctic Ocean resides (**Table 4**), are 0.15‰ lighter than inflows. However, deep waters largely lie below sill depths and are only minor contributors to the direct exchange across the gateways. Only the Fram Strait is sufficiently deep to allow bottom water exchange and there deep waters account for only about 20% of Si exported from the Arctic through the Strait (Marnela et al., 2016). The remaining export through the Fram Strait and the Canadian Archipelago is by intermediate, halocline, and PML waters that are isotopically heavier and similar in their overall isotopic composition to inflows (**Table 3** and **Figure 3**).

River inputs of dissolved Si to the Arctic Ocean stand out as having a uniquely light isotopic signature, +1.3 ± 0.3‰ (Sun et al., 2018), compared to both inflows and outflows (**Table 2**). If the isotopic similarity between inflows and outflows is correct, then this isotopically lighter input from rivers must be removed through permanent opal burial in the Arctic Ocean. Fractionation of silicic acid during diatom growth would remove lighter

isotopes from solution, eventually burying them as diatom opal in sediments. Silicon isotope values for opal from Arctic Ocean sediments are not available. However, observations of δ^{30}Si in bSi collected from the water column are entirely consistent with the sediments being a net sink for isotopically light Si. Profiles of δ^{30}Si of bSi in the central Arctic tend to show decreasing values with depth (Varela et al., 2016; Liguori et al., 2020). Values for bSi collected from deeper than 500 m average +1.16 ± 0.10‰ (n = 18, Liguori et al., 2020) and +1.5‰ (n = 1, Varela et al., 2016). Burial of this material would be consistent with the sediments being a net sink for the lighter isotopes of Si.

Liguori et al. (2020) and Varela et al. (2016) both emphasize the role of sea ice diatoms released from melting sea ice in producing the heavy isotopic signature of suspended opal relative to that of silicic acid in surface waters of the PML in the central Arctic Ocean. Sea ice diatoms tend to have heavy isotopic signatures due to the unique conditions within the brine pockets that they inhabit (Fripiat et al., 2007). However, about 75% of primary productivity in the Arctic Ocean occurs in the water column above the shelves (MacDonald et al., 2010), and shelves also account for >90% of silica production (ibid). Liguori et al. (2020) point out that the preferential removal of light Si isotopes during silica production on shelves would contribute to the heavy isotopic composition of Atlantic waters that traverse the Eurasian shelves before brine rejection induces their subduction and spread into the deep basins. In addition, the major river flows that discharge most of the annual river input of dissolved Si occur when shelves are largely ice free (Pokrovsky et al., 2013), suggesting most river Si input is processed by pelagic, rather than sea ice, diatoms in the water column on shelves consistent with the dominance of frustules of pelagic species in shelf sediments (Cremer, 1999; Astakhov et al., 2015). In section "The Polar Mixed Layer of the Central Arctic Ocean," we infer from dissolved δ^{30}Si(OH)$_4$ data that shelf production must significantly fractionate the isotopically light riverine Si sources. Such fractionation would produce exceptionally light frustules, which if buried on shelves would help balance the isotope budget for the Arctic Ocean.

Data on pore water δ^{30}Si(OH)$_4$ from the Barents Sea Shelf (Ward and Hendry, unpublished, **Table 2**) and our observations near the sea floor at station 61 suggest that the isotopic composition of Si that effluxes from sediments constitutes another input of relatively light Si to the Arctic that must be offset through opal burial. Assessing whether opal burial is sufficient to counter the impact of the input of light isotopes of Si from rivers and the benthos requires knowledge of the isotopic composition of buried opal. Suspended opal from the water column below 500 m in the central basins has a δ^{30}Si value of +1.16‰ (Liguori et al., 2020). Considering the mass and isotopic composition of dissolved Si entering the Arctic Ocean from rivers (0.41 Tmol Si a^{-1}, +1.3‰) and sediment efflux (0.39 Tmol Si a^{-1}, +1.16‰, **Table 2**) the burial of 0.16–0.30 Tmol Si with an average δ^{30}Si(OH)$_4$ of +1.16 would raise the δ^{30}Si(OH)$_4$ of the mass of Si in those combined inputs from +1.23‰ to between +1.25 and +1.28‰. The predicted values are lighter than measurements from all of the Arctic water masses (**Tables 3**, **5**) although the differences may not be significant given in the high uncertainties in the current isotope budget. Under an assumption of steady state, confirmation of this imbalance would imply the existence of additional mechanisms that remove light isotopes from the Arctic Ocean. Outflows through the Davis and Fram Straits are obvious candidates, but nether outflow appears especially light (**Tables 2**, **5**).

TABLE 5 | Estimated isotopic composition of silicic acid inflows and outflows through the Fram Strait.

Water mass	Transport[a] (Sv)	[Si(OH)]$_4$ (μmol kg^{-1})	δ^{30}Si(OH)$_4$ (‰)
Outflows			
Surface[b]	0.65	11.1 ± 2.2	+1.92 ± 0.07
DAAW	0.75	6.13 ± 0.13	+1.77 ± 0.02
uPDW	0.5	8.14 ± 0.17	+1.72 ± 0.02
CBDW + EBDW	0.3	11.87 ± 0.16	+1.64 ± 0.01
Total	2.2		
Average		8.80 ± 0.73[d]	+1.79 ± 0.08[e]
Inflows			
AW[c]	0.8	4.84 ± 0.13	+1.65 ± 0.05

[a] *Marnela et al. (2016).*
[b] *Includes PML and Halocline waters in the TPD (stations 30, 32, 38, and 43).*
[c] *Liguori et al. (2020);* ***Table 2****.*
[d] *Transport weighted average.*
[e] *Transport and mass weighted average.*

An intriguing aspect of the near linear decrease in δ^{30}Si(OH)$_4$ below the halocline in the Canada, Makarov, and Amundsen basins is that EBDW and CBDW (**Figure 8**), though heavier than deep waters in other oceans, are isotopically the lightest water masses in the Arctic Ocean (**Table 3**). They are also lighter than most of the major marine inflows (**Table 2**). These patterns, combined with the fact that the deep waters together contain half of the Si(OH)$_4$ in the Arctic Ocean (**Table 4**), raise the issue of the origin of the light isotopic signature of deep waters.

Since the dominant sources of the Arctic deep waters EBDW and CBDW are waters of Atlantic origin, mass balance allows estimation of the isotope composition of Si that accumulates in these water masses. Taking the concentration and isotopic characteristics of DAAW as a starting point (**Table 3**) suggests that the elevated [Si(OH)$_4$] and lower δ^{30}Si(OH)$_4$ of EBDW and CBDW (**Table 3**) result from the addition of Si with a δ^{30}Si(OH)$_4$ of +1.40‰ and +1.61‰, respectively. Such an isotopic composition may plausibly reflect the integrated influence of either benthic efflux or water-column dissolution of bSi. Preliminary data suggest an isotopic composition of the benthic efflux of Si to be +1.16‰ (**Table 2**) and Liguori et al. (2020) reported bSi δ^{30}Si values of +1.41‰ to +1.81‰ in the upper 500 m, and values as low as +1.14‰ in deeper waters, values that in sum would be consistent with the mass-balance calculations above. In contrast, Varela et al. (2016) report bSi δ^{30}Si in the upper 500 m ranging between +2.03‰ and +3.51‰, with a value of +1.5‰ below 500 m. Given the late-summer sampling of these two studies and the inherently variable and season-dependent nature of particulate δ^{30}Si, the relative potential of direct water-column dissolution of bSi versus addition from benthic efflux to explain the low δ^{30}Si(OH)$_4$ of Si-rich Arctic deep waters remains uncertain; nonetheless, the ultimate source of Si for both these fluxes must be the biological pumping of

isotopically light Si into the deep Arctic. Finally, we note that EBDW is both $Si(OH)_4$-poorer and isotopically lighter than CBDW, an unusual combination in a seawater context. This contrast may reflect differences in the mix of water masses contributing to deep waters in the European and Amerasian basins (Rudels, 2009) that result in the isotopic evolution of these two deep water masses from slightly different initial conditions.

The comparison of the whole-ocean and biological and biological residence times for Si in the Arctic Ocean above implied that the influence of biology is four times less in the Arctic Ocean than in the global ocean as a whole. While this weaker influence is consistent with the dominant water-mass control on the Arctic $\delta^{30}Si(OH)_4$ distribution inferred by Liguori et al. (2020), the basin-wide averaging used in those calculations masks the dichotomy between the strong biological productivity on the shallow shelves, where biological turnover times are short, compared to the lower productivity in the central Arctic Ocean that, together with the large volume of the deep basins, translates into far longer turnover times offshore. The seasonal and permanent ice cover in the Arctic likely contribute to a lower biological impact in the Arctic Ocean as they restrict the timing, duration, and spatial extent of productivity, with the majority of silica production occurring on the seasonally ice – free shelves (MacDonald et al., 2010). A lower biological impact in the Arctic Ocean overall compared to other seas would seem to suggest that the similarity in the isotopic composition of marine inflows and outflows reflects only a small influence of biological processes on the Arctic Si isotope budget; however, the analysis above suggests that the biological processing of Si is in fact a major process in the Arctic that, at least in part, compensates for the inflow of isotopically light Si from rivers and its efflux from sediments.

Some sense of the net effect of these processes comes from comparing the isotopic composition of AAW (1.76 ± 0.02‰, **Table 3**) and DAAW (+1.77 ± 0.02‰, **Table 3**) which are very similar for water masses with very different histories of interaction with productive shelf waters. AAW is derived from Atlantic water that interacts extensively with shelves (Schauer et al., 2002; Woodgate et al., 2005), while DAAW source water enters the Arctic Ocean at depth through the Fram Strait (+1.74‰, **Table 2**). It appears that shelf isotope dynamics involving freshwater inputs, silica production and sediment interactions, though significant in terms of Si fluxes, largely nullify each other's effects with respect to Si isotopes resulting in only minor alteration of isotopic composition of Atlantic inflows during their transformation into intermediate waters (**Figure 3**).

CONCLUSION

Data on the $\delta^{30}Si$ of silicic acid obtained during GN01 significantly expands the Si isotope data set for the Arctic Ocean, allowing further assessment of the processes controlling Si isotope distributions in this unique ocean. Sampling in the Bering and Chukchi Seas provided additional data on the isotopic composition of Pacific inflows, their alteration on the productive Chukchi shelf and the contribution of sediments $Si(OH)_4$ efflux in the Chukchi Sea. The light isotopic composition of Pacific waters within the UHL extended across the Canada Basin. The strength of the isotopic minimum within the double halocline of the Canada Basin was strongest in the central Canada Basin and seemed to vary with the extent of mixing between the LHL and the underlying AAW.

River inputs inferred from % meteoric waters increased both $\delta^{30}Si(OH)_4$ and $[Si(OH)_4]$ in the PML in the Canada Basin and in the TPD likely due to differences in regional biological drawdown and associated fractionation, given similarities in both $[Si(OH)_4]$ and $\delta^{30}Si(OH)_4$ for the major freshwater inputs to each region. The results also support the idea of Liguori et al. (2020) that processes within sea ice and during brine formation on the Eurasian shelves exert major controls on isotope distributions of intermediate and deep waters within the Arctic Ocean. Across all deep stations sampled, $\delta^{30}Si(OH)_4$ declined nearly linearly with depth below 275 m decreasing by only about 0.15‰ over nearly 4,000 m. The mechanisms driving this trend are unknown, but it is suggested that benthic $Si(OH)_4$ efflux plays a significant role, perhaps ultimately driven by the export of isotopically light Si in sinking bSi.

The attempted synthesis of Si isotope data from GN01, GN03/DBO15, and GN04 is the first to use reference seawater values to normalize silicon isotope data sets from multiple studies. The adjusted data span the Canada, Makarov, Amundsen, and Nansen Basins and reveal a high level of consistency among the isotopic composition of major water masses with only minor differences between water masses of common origin in the Amerasian and Eurasian Basins. Data from these expeditions confirm the observation of Varela et al. (2016) that deep waters across the Arctic Ocean are isotopically heavy compared to deep waters in all other ocean basins.

The $ALOHA_{1,000}$ – normalized data sets indicate that the isotopic composition of inflows and outflows across the major Arctic Ocean gateways are remarkably similar and suggest that Si cycling within the Arctic Ocean has little net effect on the isotope values of outflows compared to inflows, despite extensive redistribution of Si and its isotopes within the Arctic Ocean itself and significant inputs of light Si from rivers. That conclusion is quite different from that implied by a comparative analysis of unadjusted $\delta^{30}Si(OH)_4$ values, which found lighter values in the Amerasian Basin than in the Eurasian Basins, suggesting contrasting isotope signatures among the multiple outflows that eventually contribute to the isotopic signature of NADW (Liguori et al., 2020).

Biological influence on the Si cycle of the Arctic Ocean at the basin scale appears less than in the global ocean, but silica production and silica dissolution are each still dominant fluxes in the silicic acid and Si isotope budgets of the Arctic Ocean. The preferential export and sedimentary sequestration of light Si isotopes via fractionation during biological production plays a large role in compensating for the input of light river waters and light sediment pore waters into the Arctic Ocean, but additional mechanisms like the burial of exceptionally light frustules on shelves is needed to balance the isotope budget. An important role for biological production and opal dissolution in the Arctic Ocean Si isotope budget contrasts with previous suggestions of dominance of water mass mixing with only minor biological

influence in setting Si isotope distributions (Liguori et al., 2020). These inferences may be consistent with each other if the major net burial fluxes of isotopically light opal are concentrated on the shallow shelves. Confirmation of these mechanisms will require additional information on the isotopic composition across the major gateways, especially the Fram Strait and Barents Sea where direct measurements are lacking, as well as from the Eurasian and Barents Sea shelves which strongly influence the fate and characteristics of Atlantic inflows and river inputs, but where no Si isotope data exist.

DATA AVAILABILITY STATEMENT

The datasets presented in this study can be found in online repositories. The names of the repository/repositories and accession number(s) can be found below: Silicon isotope data are available at Biological and Chemical Oceanography Data Management Office (BCO-DMO) repository (Dataset version 2020-04-17). doi: 10.26008/1912/bco-dmo.809612.1; https://www.bco-dmo.org/dataset/809612. Temperature, salinity, and macronutrient data are taken from the Biological and Chemical Oceanography Data Management Office (BCO-DMO) repository (https://www.bco-dmo.org/dataset/647259).

AUTHOR CONTRIBUTIONS

MB conceived the project, designed the sampling, and wrote the manuscript. JJ, IC, and GS performed isotope analyses. CM advised on statistical handling of the data. All authors provided comments on the manuscript.

FUNDING

MB's and IC's contributions were supported by the United States National Science Foundation, Division of Ocean Sciences grant OCE-1434305. GS' and CM's contributions to this study were supported by ETH Zürich.

ACKNOWLEDGMENTS

We would like to thank the Captain and crew of the USCGC Healy; Dave Kadko and Greg Cutter for cruise leadership; Martin Fleicher for sample collection at sea; Reiner Schlitzer at AWI for use of the Ocean Data View product (https://odv.awi.de), the SIO ODF team for nutrient and salinity analyses. We thank Kate Hendry and James Ward for unpublished pore water isotopic data from the Barents Sea supported through the Changing Arctic Ocean Seafloor (ChAOS) project, part of the Changing Arctic Ocean Program funded by the Natural Environment Research Council (grant no. NE/P005942/1). GS and CM thank Werner Erni and Andreas Süsli for maintenance and repair of the mass spectrometer at ETH Zürich.

REFERENCES

Aguilar-Islas, A. M., Rember, R., Nishino, S., Kikuchi, T., and Itoh, M. (2013). Partitioning and lateral transport of iron to the Canada Basin. *Pol. Sci.* 7, 82–99. doi: 10.1016/j.polar.2012.11.001

Aksenov, Y., Ivanov, V. V., Nurser, A. J. G., Bacon, S., Polyakov, I. V., Coward, A. C., et al. (2011). The arctic circumpolar boundary current. *J. Geophys. Res. Oceans* 116:2010JC006637. doi: 10.1029/2010JC006637

Alkire, M. B., Morison, J., Schweiger, A., Zhang, J., Steele, M., Peralta-Ferriz, C., et al. (2017). A meteoric water budget for the Arctic Ocean. *J. Geophys. Res. Oceans* 122, 10020–10041. doi: 10.1002/2017jc012807

Alkire, M. B., Rember, R., and Polyakov, I. (2019). Discrepancy in the identification of the Atlantic/pacific front in the central arctic ocean: NO versus nutrient relationships. *Geophys. Res. Lett.* 46, 3843–3852. doi: 10.1029/2018GL081837

Anderson, L. G., Dyrssen, D. W., Jones, E. P., and Lowings, M. G. (1983). Inputs and outputs of salt, fresh water, alkalinity, and silica in the Arctic Ocean. *Deep Sea Res. Part A Oceanogr. Res. Pap.* 30, 87–94. doi: 10.1016/0198-0149(83)90036-5

Astakhov, A., Bosin, A., Kolesnik, A., and Obrezkova, M. (2015). Sediment geochemistry and diatom distribution in the Chukchi Sea: application for bioproductivity and paleoceanography. *Oceanography* 28, 190–201. doi: 10.5670/oceanog.2015.65

Backman, J., Jakobsson, M., Løvlie, R., Polyak, L., and Febo, L. A. (2004). Is the central Arctic Ocean a sediment starved basin? *Q. Sci. Rev.* 23, 1435–1454. doi: 10.1016/j.quascirev.2003.12.005

Beucher, C., Tréguer, P., Hapette, A.-M., Corvaisier, R., Metzl, N., and Pichon, J.-J. (2004). Intense summer Si-recycling in the surface Southern Ocean. *Geophys. Res. Lett.* 31:e018998. doi: 10.1029/2003gl018998

Beucher, C. P., Brzezinski, M. A., and Crosta, X. (2007). Silicic acid dynamics in the glacial subantarctic: implications for the silicic acid leakage hypothesis. *Glob. Biogeochem. Cycles* 21:GB3105. doi: 10.1029/2006GB002746

Beucher, C. P., Brzezinski, M. A., and Jones, J. L. (2011). Mechanisms controlling silicon isotope distribution in the Eastern Equatorial Pacific. *Geochim. Cosmochim. Acta* 75, 4286–4294.

Björk, G., and Winsor, P. (2006). The deep waters of the Eurasian Basin, Arctic Ocean: geothermal heat flow, mixing and renewal. *Deep Sea Res. Part I Oceanogr. Res. Pap.* 53, 1253–1271. doi: 10.1016/j.dsr.2006.05.006

Brown, K. A., McLaughlin, F., Tortell, P. D., Yamamoto-Kawai, M., and Francois, R. (2016). Sources of dissolved inorganic carbon to the Canada Basin halocline: a multitracer study. *J. Geophys. Res. Oceans* 121, 2918–2936. doi: 10.1002/2015jc011535

Brzezinski, M. A., and Jones, J. L. (2015). Coupling of the distribution of silicon isotopes to the meridional overturning circulation of the North Atlantic Ocean. *Deep Sea Res. Part II Top. Stud. Oceanogr.* 116, 79–88. doi: 10.1016/j.dsr2.2014.11.015

Brzezinski, M. A., Jones, J. L., Beucher, C. P., and Demarest, M. S. (2006). Automated determination of silicon isotope natural abundance by the acid decomposition of cesium hexafluosilicate. *Analyt. Chem.* 78, 6109–6114.

Brzezinski, M. A., Jones, J. L., Bidle, K., and Azam, F. (2003). The balance between silica production and silica dissolution in the sea. Insights from Monterey Bay, California applied to the global data set. *Limnol. Oceanogr.* 48, 1846–1854.

Brzezinski, M. A., Nelson, D. M., Franck, V. M., and Sigmon, D. E. (2001). Silicon dynamics within an intense open-ocean diatom bloom in the Pacific sector of the Southern Ocean. *Deep Sea Res. II* 48, 3997–4018.

Brzezinski, M. A., Villareal, T. A., and Lipschultz, F. (1998). Silica production and the contribution of diatoms to new and primary production in the central North Pacific. *Mar. Ecol. Prog. Ser.* 167, 89–104.

Cardinal, D., Alleman, L. Y., Dehairs, F., Savoye, N., Trull, T. W., and André, L. (2005). Relevance of silicon isotopes to Si-nutrient utilization and Si-source assessment in Antarctic waters. *Glob. Biogeochem. Cycles* 19:364. doi: 10.1029/2004gb002364

Carey, J. C., Gewirtzman, J., Johnston, S. E., Kurtz, A., Tang, J., Vieillard, A. M., et al. (2020). Arctic river dissolved and biogenic silicon exports—current conditions and future changes with warming. *Glob. Biogeochem. Cycles* 34:e2019GB006308. doi: 10.1029/2019gb006308

Carmack, E., and Wassmann, P. (2006). Food webs and physical–biological coupling on pan-arctic shelves: unifying concepts and comprehensive perspectives. *Prog. Oceanogr.* 71, 446–477. doi: 10.1016/j.pocean.2006.10.004

Carmack, E. C., Yamamoto-Kawai, M., Haine, T. W. N., Bacon, S., Bluhm, B. A., Lique, C., et al. (2016). Freshwater and its role in the Arctic marine system: sources, disposition, storage, export, and physical and biogeochemical consequences in the Arctic and global oceans. *J. Geophys. Res. Biogeosci.* 121, 675–717. doi: 10.1002/2015JG003140

Charette, M. A., Kipp, L. E., Jensen, L. T., Dabrowski, J. S., Whitmore, L. M., Fitzsimmons, J. N., et al. (2020). The transpolar drift as a source of riverine and shelf-derived trace elements to the central Arctic Ocean. *J. Geophys. Res. Oceans* 125:e2019JC015920. doi: 10.1029/2019jc015920

Closset, I., Cardinal, D., Rembauville, M., Thil, F., and Blain, S. (2016). Unveiling the Si cycle using isotopes in an iron-fertilized zone of the Southern Ocean: from mixed-layer supply to export. *Biogeosciences* 13, 6049–6066. doi: 10.5194/bg-13-6049-2016

Closset, I., Lasbleiz, M., Leblanc, K., Quéguiner, B., Cavagna, A. J., Elskens, M., et al. (2014). Seasonal evolution of net and regenerated silica production around a natural Fe-fertilized area in the Southern Ocean estimated with Si isotopic approaches. *Biogeosciences* 11, 5827–5846. doi: 10.5194/bg-11-5827-2014

Codispoti, L. A., and Lowman, D. (1973). A reactive silicate budget for the Arctic Ocean. *Limnol. Oceanogr.* 18, 448–456. doi: 10.4319/lo.1973.18.3.0448

Codispoti, L. A., and Owens, T. G. (1975). Nutrient transports through lancaster sound in relation to the Arctic Ocean's reactive silicate budget and the outflow of Bering Strait waters1. *Limnol. Oceanogr.* 20, 115–119. doi: 10.4319/lo.1975.20.1.0115

Cremer, H. (1999). "Spatial distribution of diatom surface sediment assemblages on the Laptev Sea Shelf (Russian Arctic)," in *Land-Ocean Systems in the Siberian Arctic*, ed. H. Kassens (Berlin: Springer).

De La Rocha, C. L., Brzezinski, M. A., and DeNiro, M. J. (1996). Purification, recovery, and laser-driven fluorination of silicon from dissolved and particulate silica for measurement of natural stable isotope abundances. *Analyt. Chem.* 68, 3746–3750.

De La Rocha, C. L., Brzezinski, M. A., and DeNiro, M. J. (1997). Fractionation of silicon isotopes by marine diatoms during bSi formation. *Geochim. Cosmochim. Acta Geochim. Cosmochim. Acta* 61, 5051–5056.

De La Rocha, C. L., Brzezinski, M. A., and DeNiro, M. J. (2000). A first look at the distribution of the stable isotopes of silicon in natural waters. *Geochim. Cosmochim. Acta* 64, 2467–2477.

De La Rocha, C. L., Brzezinski, M. A., DeNiro, M. J., and Shemesh, A. (1998). Silicon-isotope composition of diatoms as an indicator of past oceanic change. *Nature* 395, 680–683.

de Souza, G. F., Reynolds, B. C., Johnson, G. C., Bullister, J. L., and Bourdon, B. (2012a). Silicon stable isotope distribution traces Southern Ocean export of Si to the eastern South Pacific thermocline. *Biogeosciences* 9, 4199–4213.

de Souza, G. F., Reynolds, B. C., Rickli, J., Frank, M., Saito, M. A., Gerringa, L. J. A., et al. (2012b). Southern Ocean control of silicon stable isotope distribution in the deep Atlantic Ocean. *Glob. Biogeochem. Cycles* 26:GB2035. doi: 10.1029/2011gb004141

de Souza, G. F., Slater, R. D., Dunne, J. P., and Sarmiento, J. L. (2014). Deconvolving the controls on the deep ocean's silicon stable isotope distribution. *Earth Planet. Sci. Lett.* 398, 66–76. doi: 10.1016/j.epsl.2014.04.040

de Souza, G. F., Slater, R. D., Hain, M. P., Brzezinski, M. A., and Sarmiento, J. L. (2015). Distal and proximal controls on the silicon stable isotope signature of North Atlantic Deep Water. *Earth Planet. Sci. Lett.* 432, 342–353. doi: 10.1016/j.epsl.2015.10.025

Delstanche, S., Opfergelt, S., Cardinal, D., Elsass, F., André, L., and Delvaux, B. (2009). Silicon isotopic fractionation during adsorption of aqueous monosilicic acid onto iron oxide. *Geochim. Cosmochim. Acta* 73, 923–934. doi: 10.1016/j.gca.2008.11.014

Dickson, R. R., and Brown, J. (1994). The production of North Atlantic deep water: sources, rates, and pathways. *J. Geophys. Res. Oceans* 99, 12319–12341. doi: 10.1029/94JC00530

DiMento, B. P., Mason, R. P., Brooks, S., and Moore, C. (2019). The impact of sea ice on the air-sea exchange of mercury in the Arctic Ocean. *Deep Sea Res. Part I Oceanogr. Res. Pap.* 144, 28–38. doi: 10.1016/j.dsr.2018.12.001

Dumont, M., Pichevin, L., Geibert, W., Crosta, X., Michel, E., Moreton, S., et al. (2020). The nature of deep overturning and reconfigurations of the silicon cycle across the last deglaciation. *Nat. Commun.* 11:1534. doi: 10.1038/s41467-020-15101-6

Eakins, B. W., and Sharman, G. F. (2010). *Volumes of the World's Oceans from ETOPO1*. Boulder, CO: NOAA National Geophysical Data Center.

Edmonds, H. N., Michael, P. J., Baker, E. T., Connelly, D. P., Snow, J. E., Langmuir, C. H., et al. (2003). Discovery of abundant hydrothermal venting on the ultraslow-spreading Gakkel ridge in the Arctic Ocean. *Nature* 421, 252–256. doi: 10.1038/nature01351

Ehlert, C., Doering, K., Wallmann, K., Scholz, F., Sommer, S., Grasse, P., et al. (2016). Stable silicon isotope signatures of marine pore waters – Biogenic opal dissolution versus authigenic clay mineral formation. *Geochim. Cosmochim. Acta* 191, 102–117. doi: 10.1016/j.gca.2016.07.022

Ekwurzel, B., Schlosser, P., Mortlock, R. A., Fairbanks, R. G., and Swift, J. H. (2001). River runoff, sea ice meltwater, and Pacific water distribution and mean residence times in the Arctic Ocean. *J. Geophys. Res. Oceans* 106, 9075–9092. doi: 10.1029/1999jc000024

Emmerton, C. A., Lesack, L. F. W., and Vincent, W. F. (2008). Mackenzie River nutrient delivery to the Arctic Ocean and effects of the Mackenzie Delta during open water conditions. *Glob. Biogeochem. Cycles* 22:856. doi: 10.1029/2006gb002856

Fahl, K., and Nöthig, E.-M. (2007). Lithogenic and biogenic particle fluxes on the Lomonosov Ridge (central Arctic Ocean) and their relevance for sediment accumulation: vertical vs. lateral transport. *Deep Sea Res. Part I Oceanogr. Res. Pap.* 54, 1256–1272. doi: 10.1016/j.dsr.2007.04.014

Frings, P. J., Clymans, W., Fontorbe, G., De La Rocha, C. L., and Conley, D. J. (2016). The continental Si cycle and its impact on the ocean Si isotope budget. *Chem. Geol.* 425, 12–36. doi: 10.1016/j.chemgeo.2016.01.020

Fripiat, F., Cardinal, D., Tison, J.-L., Worby, A., and André, L. (2007). Diatom-induced silicon isotopic fractionation in Antarctic sea ice. *J. Geophys. Res.* 112:G02001. doi: 10.1029/2006jg000244

Fripiat, F., Cavagna, A.-J., Savoye, N., Dehairs, F., Andre, L., and Cardinal, D. (2011). Isotopic constraints on the Si-biogeochemical cycle of the Antarctic Zone in the Kerguelen area (KEOPS). *Mar. Chem.* 123, 11–22.

Fripiat, F., Meiners, K. M., Vancoppenolle, M., Papadimitriou, S., Thomas, D. N., Ackley, S. F., et al. (2017). Macro-nutrient concentrations in Antarctic pack ice: overall patterns and overlooked processes. *Elementa Sci. Anthrop.* 5:13. doi: 10.1525/elementa.217

Gao, S., Wolf Gladrow, D. A., and Volker, C. (2016). Simulating the modern δ^{30}Si distribution in the oceans and in marine sediments. *Glob. Biogeochem. Cycles* 30, 120–133. doi: 10.1002/2015GB005189

Georg, R. B., Reynolds, B. C., Frank, M., and Halliday, A. N. (2006). New sample preparation techniques for the determination of Si isotopic compositions using MC-ICPMS. *Chem. Geol.* 235, 95–104.

Giesbrecht, K. E. (2019). *Biogenic Silica Dynamics of Arctic Marine Ecosystems*. Ph.D thesis. Victoria: University of Victoria.

Grasse, P., Brzezinski, M. A., Cardinal, D., de Souza, G. F., Andersson, P., Closset, I., et al. (2017). GEOTRACES intercalibration of the stable silicon isotope composition of dissolved silicic acid in seawater. *J. Analyt. Atom. Spectrom.* 32, 562–578.

Hendry, K. R., and Brzezinski, M. A. (2014). Using silicon isotopes to understand the role of the Southern Ocean in modern and ancient biogeochemistry and climate. *Q. Sci. Rev.* 89, 13–26. doi: 10.1016/j.quascirev.2014.01.019

Hendry, K. R., Leng, M. J., Robinson, L. F., Sloane, H. J., Blusztjan, J., Rickaby, R. E. M., et al. (2011). Silicon isotopes in Antarctic sponges: an interlaboratory comparison. *Antarct. Sci.* 23, 34–42. doi: 10.1017/s0954102010000593

Holmes, R., McClelland, J., Peterson, B., Tank, S., Bulygina, E., Eglinton, T., et al. (2012). Seasonal and annual fluxes of nutrients and organic matter from large rivers to the Arctic Ocean and Surrounding Seas. *Estuar. Coasts* 35, 369–382. doi: 10.1007/s12237-011-9386-6

Holmes, R. M., McClelland, J. W., Tank, S. E., Spencer, R. G. M., and Shiklomanov, A. I. (2021). *Arctic Great Rivers Observatory. Water Quality Dataset, Version*

20210608. Available online at: https://www.arcticgreatrivers.org/data (accessed June, 2021).

Holzer, M., and Brzezinski, M. A. (2015). Controls on the silicon isotope distribution in the ocean: new diagnostics from a data-constrained model. *Glob. Biogeochem. Cycles* 29, 267–287. doi: 10.1002/2014gb004967

Hydes, D. J., Aoyama, M., Aminot, A., Bakker, K., Becker, S., Coverly, S., et al. (2010). "Determination of dissolved nutrients (N, P, SI) in seawater with high precision and inter-comparability using gas-segmented continuous flow analysers," in *The GO-SHIP Repeat Hydrography Manual: A Collection of Expert Reports and Guidelines. Version 1, IOCCP Report Number 14, ICPO Publication Series Number 134*, eds E. M. Hood, C. L. Sabine, and B. M. Sloyan (Kristineberg: IOCCP).

Jensen, L. T., Wyatt, N. J., Twining, B. S., Rauschenberg, S., Landing, W. M., Sherrell, R. M., et al. (2019). Biogeochemical cycling of dissolved zinc in the Western Arctic (Arctic GEOTRACES GN01). *Glob. Biogeochem. Cycles* 33, 343–369. doi: 10.1029/2018gb005975

Jones, E. P., and Anderson, L. G. (1986). On the origin of the chemical properties of the Arctic Ocean halocline. *J. Geophys. Res. Oceans* 91, 10759–10767. doi: 10.1029/JC091iC09p10759

Jones, E. P., and Coote, A. R. (1980). Nutrient distributions in the Canadian Archipelago: indicators of summer water mass and flow characteristics. *Can. J. Fish. Aquat. Sci.* 37, 589–599. doi: 10.1139/f80-075

Kipp, L. E., Spall, M. A., Pickart, R. S., Kadko, D. C., Moore, W. S., Dabrowski, J. S., et al. (2020). Observational and modeling evidence of seasonal trends in sediment-derived material inputs to the Chukchi Sea. *J. Geophys. Res. Oceans* 125:e2019JC016007. doi: 10.1029/2019JC016007

Leo, W. R. (1994). *Techniques for Nuclear and Particle Physics Experiments*, 2nd Edn, Berlin: Springer-Verlag.

Lewin, J. C. (1962). "Silicification," in *Physiology and Biochemistry of Algae*, ed. R. A. Lewin (New York, NY: Academic Press), 445–455.

Li, J., Pickart, R. S., Lin, P., Bahr, F., Arrigo, K. R., Juranek, L., et al. (2020). The Atlantic water boundary current in the Chukchi Borderland and Southern Canada Basin. *J. Geophys. Res. Oceans* 125:e2020JC016197. doi: 10.1029/2020jc016197

Liguori, B. T. P., Ehlert, C., and Pahnke, K. (2020). The influence of water mass mixing and particle dissolution on the silicon cycle in the Central Arctic Ocean. *Front. Mar. Sci.* 7:202. doi: 10.3389/fmars.2020.00202

MacDonald, R. W., Anderson, L. G., Christensen, J. P., Miller, L. A., Semiletov, I. P., and Stein, R. (2010). "The Arctic Ocean," in *Carbon and Nutrient Fluxes in Continental Margins*, ed. K. K. Liu (Berlin: Sperling-Verlag), 292–303.

Marnela, M., Rudels, B., Goszczko, I., Beszczynska-Möller, A., and Schauer, U. (2016). Fram Strait and Greenland Sea transports, water masses, and water mass transformations 1999–2010 (and beyond). *J. Geophys. Res. Oceans* 121, 2314–2346. doi: 10.1002/2015jc011312

März, C., Meinhardt, A. K., Schnetger, B., and Brumsack, H. J. (2015). Silica diagenesis and benthic fluxes in the Arctic Ocean. *Mar. Chem.* 171, 1–9. doi: 10.1016/j.marchem.2015.02.003

McClelland, J. W., Holmes, R. M., Dunton, K. H., and Macdonald, R. W. (2012). The Arctic Ocean Estuary. *Estuar. Coasts* 35, 353–368. doi: 10.1007/s12237-010-9357-3

Middag, R., de Baar, H. J. W., Laan, P., and Bakker, K. (2009). Dissolved aluminium and the silicon cycle in the Arctic Ocean. *Mar. Chem.* 115, 176–195. doi: 10.1016/j.marchem.2009.08.002

Nelson, D. M., Ahern, J. A., and Herlihy, L. J. (1991). Cycling of biogenic silica within the upper water column of the Ross Sea. *Mar. Chem.* 35, 461–476.

Nelson, D. M., and Brzezinski, M. A. (1997). Diatom growth and productivity in an oligotrophic midocean gyre: a 3-yr record from the Sargasso Sea near Bermuda. *Limnol. Oceanogr.* 42, 473–486.

Newton, R., Schlosser, P., Mortlock, R., Swift, J., and MacDonald, R. (2013). Canadian Basin freshwater sources and changes: results from the 2005 Arctic Ocean Section. *J. Geophys. Res. Oceans* 118, 2133–2154. doi: 10.1002/jgrc.20101

Nishino, S., Kawaguchi, Y., Inoue, J., Hirawake, T., Fujiwara, A., Futsuki, R., et al. (2015). Nutrient supply and biological response to wind-induced mixing, inertial motion, internal waves, and currents in the northern Chukchi Sea. *J. Geophys. Res. Oceans* 120, 1975–1992. doi: 10.1002/2014JC010407

Nishino, S., Shimada, K., Itoh, M., and Chiba, S. (2009). Vertical double silicate maxima in the sea-ice reduction region of the western Arctic Ocean: implications for an enhanced biological pump due to sea-ice reduction. *J. Oceanogr.* 65, 871–883. doi: 10.1007/s10872-009-0072-2

Opfergelt, S., and Delmelle, P. (2012). Silicon isotopes and continental weathering processes: assessing controls on Si transfer to the ocean. *Compt. Rendus Geosci.* 344, 723–738. doi: 10.1016/j.crte.2012.09.006

Paffrath, R., Laukert, G., Bauch, D., Rutgers van der Loeff, M., and Pahnke, K. (2021). Separating individual contributions of major Siberian rivers in the Transpolar Drift of the Arctic Ocean. *Sci. Rep.* 11:8216. doi: 10.1038/s41598-021-86948-y

Paul, D., Skrzypek, G., and Fórizs, I. (2007). Normalization of measured stable isotopic compositions to isotope reference scales – a review. *Rapid Commun. Mass Spectrom.* 21, 3006–3014. doi: 10.1002/rcm.3185

Pokrovsky, O. S., Reynolds, B. C., Prokushkin, A. S., Schott, J., and Viers, J. (2013). Silicon isotope variations in Central Siberian rivers during basalt weathering in permafrost-dominated larch forests. *Chem. Geol.* 355, 103–116. doi: 10.1016/j.chemgeo.2013.07.016

Reynolds, B. C. (2009). Modeling the modern marine δ^{30}Si distribution. *Glob. Biogeochem. Cycles* 23:GB2015. doi: 10.1029/2008GB003266

Reynolds, B. C., Aggarwal, J., Andre, L., Baxter, D., Beucher, C., Brzezinski, M. A., et al. (2007). An inter-laboratory comparison of Si isotope reference materials. *J. Analyt. Atom. Spectrom.* 22, 561–568.

Reynolds, B. C., Frank, M., and Halliday, A. N. (2006). Silicon isotope fractionation during nutrient utilization in the North Pacific. *Earth Planet. Sci. Lett.* 244, 431–443.

Rudels, B. (2009). "Arctic Ocean circulation," in *Encyclopedia of Ocean Science*, eds J. Steele, S. Thorpe, and K. Turekian (Cambridge, MA: Academic Press), 211–225.

Rudels, B. (2012). Arctic Ocean circulation and variability advection and external forcing encounter constraints and local processes. *Ocean Sci.* 8, 261–286. doi: 10.5194/os-8-261-2012

Rudels, B., Björk, G., Nilsson, J., Winsor, P., Lake, I., and Nohr, C. (2005). The interaction between waters from the Arctic Ocean and the Nordic Seas north of Fram Strait and along the East Greenland current: results from the Arctic Ocean-02 Oden expedition. *J. Mar. Syst.* 55, 1–30. doi: 10.1016/j.jmarsys.2004.06.008

Rudels, B., Korhonen, M., Schauer, U., Pisarev, S., Rabe, B., and Wisotzki, A. (2015). Circulation and transformation of Atlantic water in the Eurasian Basin and the contribution of the Fram Strait inflow branch to the Arctic Ocean heat budget. *Prog. Oceanogr.* 132, 128–152. doi: 10.1016/j.pocean.2014.04.003

Schauer, U., Rudels, B., Jones, E. P., Anderson, L. G., Muench, R. D., Björk, G., et al. (2002). Confluence and redistribution of Atlantic water in the Nansen, Amundsen and Makarov basins. *Ann. Geophys.* 20, 257–273. doi: 10.5194/angeo-20-257-2002

Schlosser, P., Kromer, B., Ekwurzel, B., Bönisch, G., McNichol, A., Schneider, R., et al. (1997). The first trans-Arctic 14C section. Comparison of the mean ages of the deep waters in the Eurasian and Canadian basins of the Arctic Ocean. *Nuclear Instrum. Methods Phys. Res. Sect. B Beam Interact. Mater. Atoms* 123, 431–437. doi: 10.1016/s0168-583x(96)00677-5

Schauer, U., Muench, R. D., Rudels, B., and Timokhov, L. (1997). Impact of eastern Arctic shelf waters on the Nansen Basin intermediate layers. *J. Geophys. Res. Oceans* 102, 3371–3382. doi: 10.1029/96JC03366

Shimada, K., Itoh, M., Nishino, S., McLaughlin, F., Carmack, E., and Proshutinsky, A. (2005). Halocline structure in the Canada Basin of the Arctic Ocean. *Geophys. Res. Lett.* 32:L03605. doi: 10.1029/2004gl021358

Sun, X., Mörth, C.-M., Porcelli, D., Kutscher, L., Hirst, C., Murphy, M. J., et al. (2018). Stable silicon isotopic compositions of the Lena River and its tributaries: implications for silicon delivery to the Arctic Ocean. *Geochim. Cosmochim. Acta* 241, 120–133. doi: 10.1016/j.gca.2018.08.044

Sutton, J. N., de Souza, G. F., García-Ibáñez, M. I., and De La Rocha, C. L. (2018). The silicon stable isotope distribution along the GEOVIDE section (GEOTRACES GA-01) of the North Atlantic Ocean. *Biogeosciences* 15, 5663–5676. doi: 10.5194/bg-15-5663-2018

Swift, J. H., Jones, E. P., Aagaard, K., Carmack, E. C., Hingston, M., MacDonald, R. W., et al. (1997). Waters of the makarov and canada basins. *Deep Sea Res. 2 Top. Stud. Oceanogr.* 44, 1503–1529. doi: 10.1016/S0967-0645(97)00055-6

Tanhua, T., Jones, E. P., Jeansson, E., Jutterström, S., Smethie, W. M. Jr., Wallace, D. W. R., et al. (2009). Ventilation of the Arctic Ocean: mean ages and inventories of anthropogenic CO_2 and CFC-11. *J. Geophys. Res. Oceans* 114:e2008JC004868. doi: 10.1029/2008jc004868

Timmermans, M.-L., Garrett, C., and Carmack, E. (2003). The thermohaline structure and evolution of the deep waters in the Canada Basin, Arctic Ocean. *Deep Sea Res. Part I Oceanogr. Res. Pap.* 50, 1305–1321. doi: 10.1016/S0967-0637(03)00125-0

Torres-Valdés, S., Tsubouchi, T., Bacon, S., Naveira-Garabato, A. C., Sanders, R., McLaughlin, F. A., et al. (2013). Export of nutrients from the Arctic Ocean. *J. Geophys. Res. Oceans* 118, 1625–1644. doi: 10.1002/jgrc.20063

Tovar-Sánchez, A., Duarte, C. M., Alonso, J. C., Lacorte, S., Tauler, R., and Galbán-Malagón, C. (2010). Impacts of metals and nutrients released from melting multiyear Arctic sea ice. *J. Geophys. Res. Oceans* 115:e2009JC005685. doi: 10.1029/2009JC005685

Tréguer, P., and van Bennekom, A. J. (1991). The annual production of biogenic silica in the Antarctic Ocean. *Mar. Chem.* 35, 477–487.

Tréguer, P. J., and De La Rocha, C. L. (2013). The world ocean silica cycle. *Annua. Rev. Mar. Sci.* 5, 477–501. doi: 10.1146/annurev-marine-121211-172346

Tréguer, P. J., Sutton, J. N., Brzezinski, M., Charette, M. A., Devries, T., Dutkiewicz, S., et al. (2021). Reviews and syntheses: the biogeochemical cycle of silicon in the modern ocean. *Biogeosciences* 18, 1269–1289. doi: 10.5194/bg-18-1269-2021

Uchimiya, M., Motegi, C., Nishino, S., Kawaguchi, Y., Inoue, J., Ogawa, H., et al. (2016). Coupled response of bacterial production to a wind-induced fall phytoplankton bloom and sediment Resuspension in the Chukchi Sea Shelf, Western Arctic Ocean. *Front. Mar. Sci.* 3:231. doi: 10.3389/fmars.2016.00231

Varela, D. E., Brzezinski, M. A., Beucher, C. P., Jones, J. L., Giesbrecht, K. E., Lansard, B., et al. (2016). Heavy silicon isotopic composition of silicic acid and biogenic silica in Arctic waters over the Beaufort shelf and the Canada Basin. *Glob. Biogeochem. Cycles* 30, 804–824. doi: 10.1002/2015gb005277

Varela, D. E., Pride, C. J., and Brzezinski, M. A. (2004). Biological fractionation of silicon isotopes in Southern Ocean surface waters. *Glob. Biogeochem. Cycles* 18:GB1047.

Wassmann, P. (2015). Overarching perspectives of contemporary and future ecosystems in the Arctic Ocean. *Prog. Oceanogr.* 139, 1–12. doi: 10.1016/j.pocean.2015.08.004

Whitmore, L. M., Pasqualini, A., Newton, R., and Shiller, A. M. (2020). Gallium: a new tracer of pacific water in the Arctic ocean. *J. Geophys. Res. Oceans* 125:e2019JC015842. doi: 10.1029/2019jc015842

Woodgate, R., Aagaard, K., Swift, J., Falkner, K., and Smethie, W. (2005). Pacific ventilation of the Artic Ocean's lower halocline by upwelling and diapycnal mixing over the continental margin. *Geophys. Res. Lett.* 32:e2005GL023999. doi: 10.1029/2005gl023999

Woodgate, R. A., Aagaard, K., Muench, R. D., Gunn, J., Bjork, G., Rudels, B., et al. (2001). The Arctic Ocean boundary current along the Eurasian slope and the adjacent Lomonosov Ridge: water mass properties, transports and transformations from moored instruments. *Deep Sea Res. Part 1 Oceanogr. Res. Pap.* 48, 1757–1792.

Xiang, Y., and Lam, P. J. (2020). Size-fractionated compositions of marine suspended particles in the Western Arctic Ocean: lateral and vertical sources. *J. Geophys. Res. Oceans* 125:e2020JC016144. doi: 10.1029/2020JC016144

Zhang, R., Jensen, L. T., Fitzsimmons, J. N., Sherrell, R. M., and John, S. (2019). Dissolved cadmium and cadmium stable isotopes in the western Arctic Ocean. *Geochim. Cosmochim. Acta* 258, 258–273. doi: 10.1016/j.gca.2019.05.028

Zheng, X.-Y., Beard, B. L., Reddy, T. R., Roden, E. E., and Johnson, C. M. (2016). Abiologic silicon isotope fractionation between aqueous Si and Fe(III)–Si gel in simulated Archean seawater: implications for Si isotope records in Precambrian sedimentary rocks. *Geochim. Cosmochim. Acta* 187, 102–122. doi: 10.1016/j.gca.2016.05.012

Conflict of Interest: The authors declare that the research was conducted in the absence of any commercial or financial relationships that could be construed as a potential conflict of interest.

Publisher's Note: All claims expressed in this article are solely those of the authors and do not necessarily represent those of their affiliated organizations, or those of the publisher, the editors and the reviewers. Any product that may be evaluated in this article, or claim that may be made by its manufacturer, is not guaranteed or endorsed by the publisher.